



# Low-order continualization of an anisotropic membrane lattice with next-nearest interactions. Enhanced prediction of its dynamic behaviour

F. Gómez-Silva\*, R. Zaera

Department of Continuum Mechanics and Structural Analysis, University Carlos III of Madrid, Avda. de la Universidad, 30. 28911 Leganés, Madrid, Spain

## ARTICLE INFO

### Keywords:

Membrane lattice  
Next-nearest interactions  
Dispersive behaviour  
Continualization  
Pseudo-differential operator  
Natural frequencies

## ABSTRACT

In this paper, a novel anisotropic membrane lattice with nearest and next-nearest interactions (long-range forces) has been continualized through different standard and non-standard continualization procedures, which enables the development of new non-classical continuum models capable of accurately capturing the scale effects, present in the matter due to its discrete nature. The performance of these continuum models is assessed by means of both dispersion and natural frequencies analyses, where the discrete model is considered as a reference. In addition, the appearance of certain physical inconsistencies in some of the developed models is analysed, concluding that these only appear for those developed with continualizations based on Taylor expansion. Interestingly, the non-standard models suitably capture the dispersive behaviour of the discrete one, without both physical inconsistencies and higher-order spatial derivatives, thus avoiding the need for extra boundary conditions when finite solids are involved.

## 1. Introduction

It is well known that matter is essentially discrete, presenting internal structures that can influence its dynamic behaviour. This phenomenon is known as *size-effect*, and can arise in several problems, where materials with a significant internal structure are involved, thus leading to the occurrence of characteristic lengths that introduce a size dependence in the behaviour of the solid. This characteristic length is not accounted by classical continuum models (failing in this type of problems), and may be present in micro- and nano-scale engineering problems using nano- and micro-electromechanical systems (Rahmani et al., 2022; Papkova et al., 2022), such as robotics (Braun et al., 2005; Yin et al., 2021) and biosensing (Eom et al., 2011; Caldas et al., 2017), as well as in macro-scale problems, such as metamaterials (Lee et al., 2017; Zaera et al., 2018; Dunn and Wheel, 2020) and composites (Wisnom, 1999; Rafiee et al., 2017; Civalcek et al., 2021).

These size-effects can be accurately captured by means of discrete models, which address each element of the internal structure individually, this meaning that a higher calculation cost is required to solve them (large number of degrees of freedom). This is why Cauchy and Voigt in the 19th century, and Cosserat brothers at the beginning of the 20th century developed non-classical continuum models, capable of capturing the size-effects with a lower calculation cost. In the 1960s these models made a comeback with works carried out by Mindlin (1963), Toupin (1962) or Eringen (1966), Eringen and Edelen (1972), among others. Nonetheless, the interest in this issue is still ongoing

today, with recent works based, among others, on the strain gradient elasticity or on the modified couple stress theories, which are widely implemented to solve problems concerning rods (Khakalo and Niiranen, 2018; Barretta et al., 2019), beams (Zhang et al., 2020; Abdelrahman et al., 2021), membranes (Shang et al., 2019; Harbola et al., 2021) or plates (Thai et al., 2018; Liu et al., 2021). However, all these models are considered axiomatic, and therefore depend on non-classical parameters, whose value must be determined by experimental tests. For this reason, the *continualization* of discrete lattice systems emerges as an alternative. These systems consist of periodically repeated cells, and by applying continualization methods to them, non-classical continuum models are derived, whose scale parameters are linked to the geometrical and mechanical properties of the lattice.

The Born–von Kármán or Lagrange lattice (see Andrianov et al. (2021) for more details on this naming) is the simplest system for understanding the size-effects in the discrete media. This lattice consists of a chain formed by particles and springs that undergo deformation when the particles are longitudinally displaced. Different standard (based on Taylor expansions) continualization techniques were applied to it by Polyzos and Fotiadis (2012), thus yielding to non-classical continuum models with high-order differential equations. On the other hand, non-standard continualization procedures (based on pseudo-differential operators) have been widely employed in order to avoid these high-order derivatives, such as the use of an enriched kinetic energy, proposed by Rosenau (2003), or the *Regularization* technique suggested by

\* Corresponding author.

E-mail address: [frgomezs@ing.uc3m.es](mailto:frgomezs@ing.uc3m.es) (F. Gómez-Silva).

Bacigalupo and Gambarotta (2019). Challamel et al. (2018) consider a variant of this lattice in order to reproduce the Eringen's nonlocal model. Andrianov et al. apply a continualization approach based on the composite equations to both one-dimensional (Andrianov and Awrejcewicz, 2003; Andrianov, 2002; Andrianov and Awrejcewicz, 2005) and two-dimensional (Andrianov et al., 2010) lattice systems with nearest interactions. In Andrianov and Awrejcewicz (2005, 2008), they also employ two-point Padé approximants for the continualization of this kind of lattices, reaching similar results. Nonetheless, the application of the two-point Padé technique to lattice systems with next-nearest interactions cancels the contribution of springs connecting next-nearest neighbours when saw-tooth oscillations are imposed in the limiting case (short-wavelength propagation at the limit of the Irreducible Brillouin Zone), thus resulting in the same continuum models derived when only nearest interactions are considered. A lattice system like the Born–von Kármán lattice, but including next-nearest interactions is studied by Gómez-Silva et al. (2020) and Gómez-Silva and Zaera (2022b), applying to it several standard and non-standard continualization methods. The idea of including next-nearest interactions in lattice systems was proposed by Gazis and Wallis (1965), Mindlin (1965) and Rosenau (1987), among others, which arises from non-local theories of long-range forces suggested by Eringen and Edelen (1972) in the early 1970s, with the aim of capturing some unexpected performances observed in experimental tests. Di Paola et al. (2010) consider a lattice system with multiple neighbours interactions, where the stiffness of the springs decays with distance.

Lattice beams systems, considering bending deformation through rotational springs, have been also studied by Wang et al. (2013), Challamel et al. (2014), Hache et al. (2017) and Gómez-Silva and Zaera (2021). Shear deformations can be also considered by including transverse springs, as it is suggested in Zhang et al. (2013), Duan et al. (2013), Gómez-Silva and Zaera (2022a), thus deriving non-classical Timoshenko beam models.

In the context of membranes, lattice systems with nearest interactions have been explored in the last years with works such as that of Andrianov and Awrejcewicz (2008), who employ a standard continualization method, or such as of Lombardo and Askes (2010) and Hérisson et al. (2018), which also propose a non-standard continualization procedure using Padé approximants. In these works, both dispersion relations and natural frequencies of the discrete model are studied. However, the governing equations of the non-classical continuum models obtained in these works present high-order spatial derivatives, which means that they need extra boundary conditions to be solved when finite (bounded) solids are treated, whose meaning is unclear. This issue was addressed by Rosenau (1987), who reached a low-order continuum model by employing Schrödinger operators. Bacigalupo and Gambarotta (2021) employ the Regularization method, leading to a non-classical model that captures the size-effects though cross space–time derivatives with low spatial order. Andrianov and Awrejcewicz (2008) suggest an approach based on two-points Padé approximants for the continualization of a membrane lattice with nearest interactions, which also leads to a low-order continuum model. Gómez-Silva and Zaera (2022) analysed an anisotropic membrane lattice, applying to it several standard and non-standard continualization procedures, and performing an analysis of both dispersion relations and natural frequencies, identifying the correlations between them. On the other hand, Zaera et al. (2018) proposed a square nonlinear membrane lattice, formed by particles linked to each other by means of linear springs and to the ground by nonlinear ones. They employed standard continualization method, investigating the existence of solitary waves.

In this paper, a novel anisotropic (establishing a spring stiffness ratio in  $x$  and  $y$  directions) membrane lattice, considering next-nearest interactions is proposed. Several standard and non-standard continualization methods are applied, looking for new non-classical continuum models that do not include higher-order spatial derivatives in their

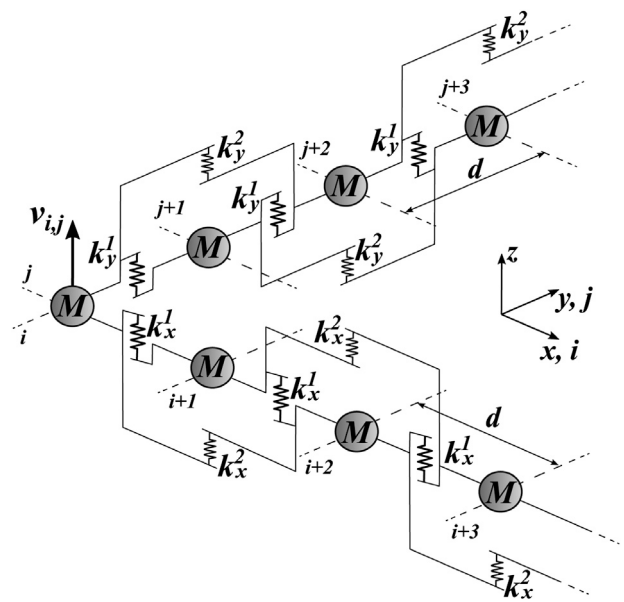


Fig. 1. Discrete reference model. Lattice made up of periodic square cells with dimensions  $d \times d$ .

governing equations. The ability of these new non-classical continuum models in capturing the size-effects is evaluated by comparing their dynamic behaviour with that of the discrete one, taken as a reference. For this purpose, dispersion relations as well as natural frequencies for a *fixed-edge* configuration are analysed for square and rectangular membranes. The correlation between both dispersion and natural frequencies analysis is provided, examining the influence of the next-nearest interactions. In addition, the occurrence of physical inconsistencies in some of these new models is discussed.

This paper is structured as follows. The Section 2 introduces the discrete reference model, founding its dispersion relation, and analysing the influence of the next-nearest interactions. Subsequently, several standard and non-standard continualization methods are applied in Section 3 to the discrete model, thus obtaining novel non-classical continuum models and their corresponding dispersion relations. In Section 4, finite solids are treated by means of a natural frequencies analysis of the *fixed-edge* configuration for both discrete and low-order continuum models. Then, a discussion of the results is presented in Section 5, evaluating the capability of the continuum models in capturing the behaviour of the discrete one, as well as examining the appearance of certain physical inconsistencies. Finally, the conclusions drawn from this work are set out in Section 6.

## 2. Discrete reference model

In this section, the rectangular lattice system, which is going to be considered as a reference, is presented. Fig. 1 shows some of the particles that constitute the lattice, which are repeatedly assembled at equal distance  $d$  (considered as a characteristic length) in  $x$  and  $y$  directions. Therefore, the lattice system is made up of a set of particles with mass  $M$  that covers an area  $L_x \times L_y = (dN_x) \times (dN_y)$ , where  $N_x$  and  $N_y$  are the number of spaces between particles in  $x$  and  $y$  directions, respectively. These particles are connected to their nearest neighbours in  $x$  and  $y$  directions by means of elastic linear springs of stiffness  $k_x^1$  and  $k_y^1$ , respectively. In addition, each particle is also linked to their next-nearest neighbour in  $x$  and  $y$  directions through secondary linear springs of stiffness  $k_x^2$  and  $k_y^2$ , respectively. Both types of springs undergo strain in  $z$  direction, so they provide a resorting force in that direction, which is proportional to the relative vertical displacement between particles, this displacement being  $v_{i,j}$ ,

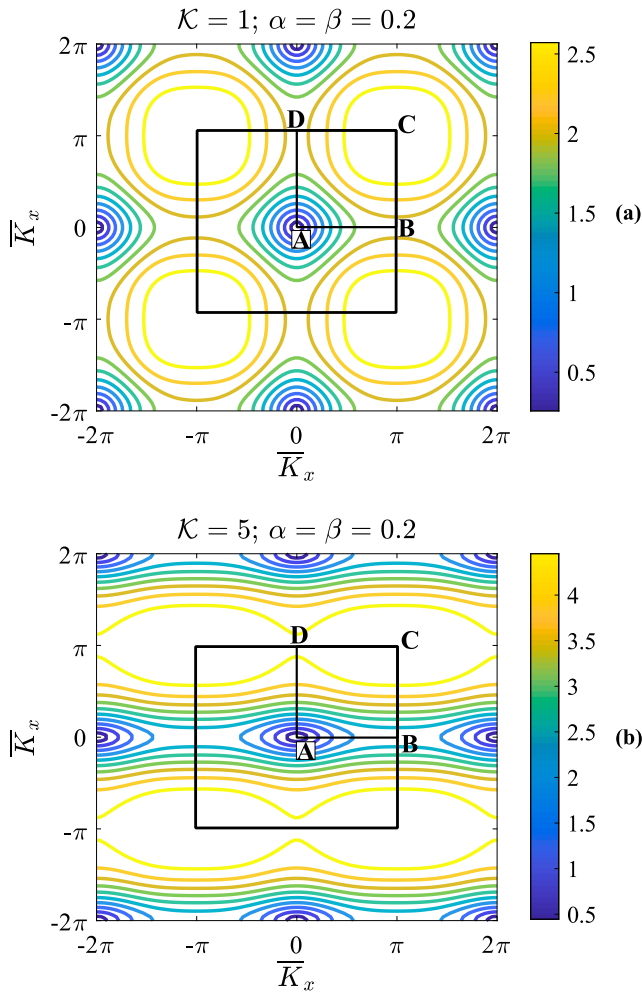


**Fig. 2.** Iso-frequency contours corresponding to the dispersion relations of the discrete model with  $\alpha = \beta = 0.2$  (value of the dimensionless frequency  $\Omega$  given by the colour scale). Irreducible Brillouin Zone delimited by the square of vertices A, B, C y D. (a)  $\mathcal{K} = 1$ . (b)  $\mathcal{K} = 5$ .

$i = 0, \dots, N_x, j = 0, \dots, N_y$ . On the other hand, the position of each particle can be defined in the plane by  $x_i = id, i = 0, \dots, N_x$  and  $y_j = jd, j = 0, \dots, N_y$ . Taking into account the previous considerations, the elastic potential energy of the whole system can be defined as

$$W = \frac{1}{2} \sum_{i=0}^{N_x-1} \sum_{j=0}^{N_y} k_x^1 (v_{i+1,j} - v_{i,j})^2 + \frac{1}{2} \sum_{i=0}^{N_x} \sum_{j=0}^{N_y-1} k_y^1 (v_{i,j+1} - v_{i,j})^2 + \frac{1}{2} \sum_{i=0}^{N_x-2} \sum_{j=0}^{N_y} k_x^2 (v_{i+2,j} - v_{i,j})^2 + \frac{1}{2} \sum_{i=0}^{N_x} \sum_{j=0}^{N_y-2} k_y^2 (v_{i,j+2} - v_{i,j})^2, \quad (1)$$

whereas the total kinetic energy results

$$T = \frac{1}{2} M \sum_{i=0}^{N_x} \sum_{j=0}^{N_y} \left( \frac{\partial v_{i,j}}{\partial t} \right)^2. \quad (2)$$

Knowing that the Lagrangian of the system is defined by  $\mathcal{L} = T - W$ , and employing the Euler–Lagrange equation

$$\frac{\partial \mathcal{L}}{\partial v_{i,j}} = \frac{d}{dt} \left( \frac{\partial \mathcal{L}}{\partial \dot{v}_{i,j}} \right), \quad (3)$$

where  $(\dot{\phantom{v}})$  corresponds to the time derivative, the following governing equation for the discrete model is reached

$$k_x^1 (v_{i+1,j} - 2v_{i,j} + v_{i-1,j}) + k_y^1 (v_{i,j+1} - 2v_{i,j} + v_{i,j-1}) + k_x^2 (v_{i+2,j} - 2v_{i,j} + v_{i-2,j}) + k_y^2 (v_{i,j+2} - 2v_{i,j} + v_{i,j-2}) = M \frac{\partial^2 v_{i,j}}{\partial t^2}, \quad (4)$$

which can be rewritten in dimensionless form as

$$(\bar{v}_{i+1,j} - 2\bar{v}_{i,j} + \bar{v}_{i-1,j}) + \mathcal{K}(\bar{v}_{i,j+1} - 2\bar{v}_{i,j} + \bar{v}_{i,j-1}) + \alpha(\bar{v}_{i+2,j} - 2\bar{v}_{i,j} + \bar{v}_{i-2,j}) + \beta\mathcal{K}(\bar{v}_{i,j+2} - 2\bar{v}_{i,j} + \bar{v}_{i,j-2}) = \frac{\partial^2 \bar{v}_{i,j}}{\partial \tau^2}, \quad (5)$$

where

$$\bar{v}_{i,j} = \frac{v_{i,j}}{d}; \quad \tau = t\tilde{\omega}; \quad \tilde{\omega} = \sqrt{\frac{k_x^1}{M}}; \quad \mathcal{K} = \frac{k_y^1}{k_x^1}; \quad \alpha = \frac{k_x^2}{k_x^1}; \quad \beta = \frac{k_y^2}{k_y^1}. \quad (6)$$

The dispersion equation of the discrete model can be obtained by assuming the following plane wave as a solution of Eq. (5)

$$\bar{v}_{i,j}(\tau) = V e^{i(\bar{K}_x \bar{x}_i + \bar{K}_y \bar{y}_j - \Omega \tau)}, \quad (7)$$

where  $V$  is the amplitude, and  $\bar{K}_x = K_x d, \bar{K}_y = K_y d$  and  $\Omega = \omega/\tilde{\omega}$  are the dimensionless wavenumber in  $x$  and  $y$  directions and the dimensionless frequency, respectively,  $K_x, K_y$  and  $\omega$  being their respective dimensional counterparts. On the other hand,  $\bar{x}_i = x_i/d = i, i = 0, \dots, N_x$  and  $\bar{y}_j = y_j/d = j, j = 0, \dots, N_y$  refer to the dimensionless discrete position variables corresponding to the particle  $i, j$ . Therefore, introducing Eq. (7) in Eq. (5), the next dispersion relation is obtained

$$\Omega = \sqrt{2 \left[ (1 - \cos(\bar{K}_x)) + \mathcal{K}(1 - \cos(\bar{K}_y)) + \alpha(1 - \cos(2\bar{K}_x)) + \beta\mathcal{K}(1 - \cos(2\bar{K}_y)) \right]}, \quad (8)$$

which states the relation between frequency and wavenumber, depending on the dimensionless parameters  $\mathcal{K}, \alpha$  and  $\beta$ . Note that these parameters are always positive,  $\alpha$  and  $\beta$  providing the ratio between the stiffness of the springs connecting the nearest and the next-nearest particles, whose value must be  $\alpha \geq -1/4$  and  $\beta \geq -1/4$ , since lower values of these parameters would lead to the appearance of imaginary frequencies, which does not make sense in a lattice like the one considered here (see Kunin (2012) for more details on this type of restrictions in lattices with next-nearest interactions). On the other hand, due to the fact that the interaction force between particles decays with distance (Di Paola et al., 2010), it can be considered that the value of  $k_x^1$  and  $k_y^1$  is significantly higher than that of  $k_x^2$  and  $k_y^2$ , respectively. Furthermore, in practical cases it is common to consider only positive values of these parameters, so in this paper we consider that  $0 \leq \alpha = \beta \leq 0.2$ , assuming the same value for both parameters for simplicity.

As an illustrative example, Fig. 2 shows the dispersion relation of a lattice with  $\alpha = \beta = 0.2$ , for  $\mathcal{K} = 1$  and  $\mathcal{K} = 5$ . In this figure, the surface defined by Eq. (8) is presented in form of iso-frequency contours. It can be seen how for  $\mathcal{K} = 1$ , Fig. 2(a), the shape of the iso-frequency contours is circular for low wavenumbers, it meaning isotropic character, which disappears for high wavenumbers. However, in the case of  $\mathcal{K} = 5$ , Fig. 2(b), the anisotropic character of the lattice is emphasized, the shape of the iso-frequency contours not presenting circular shape even for very low wavenumbers. Notice how the dispersion relation is periodic in both  $x$  and  $y$  directions, with period  $2\pi$ , it being symmetric with respect to the axes  $\bar{K}_x = \pi$  and  $\bar{K}_y = \pi$ . For this reason, only the study of dispersion relation in the Irreducible Brillouin Zone (IBZ) is of interest, this being enclosed by the square of vertices A, B, C and D in Fig. 2 ( $0 < \bar{K}_x < \pi; 0 < \bar{K}_y < \pi$ ). Moreover, the iso-frequency contour shows symmetry with respect to the straight line between vertices A and C when  $\mathcal{K} = 1$ , feature that disappears for  $\mathcal{K} = 5$ .

In order to analyse the dispersion relation in the IBZ, it is plotted along the edges A-B-C-D-A in Fig. 3. Both  $\mathcal{K} = 1$  and  $\mathcal{K} = 5$  cases have been considered, for different values of  $\alpha$ . Note how both cases agree

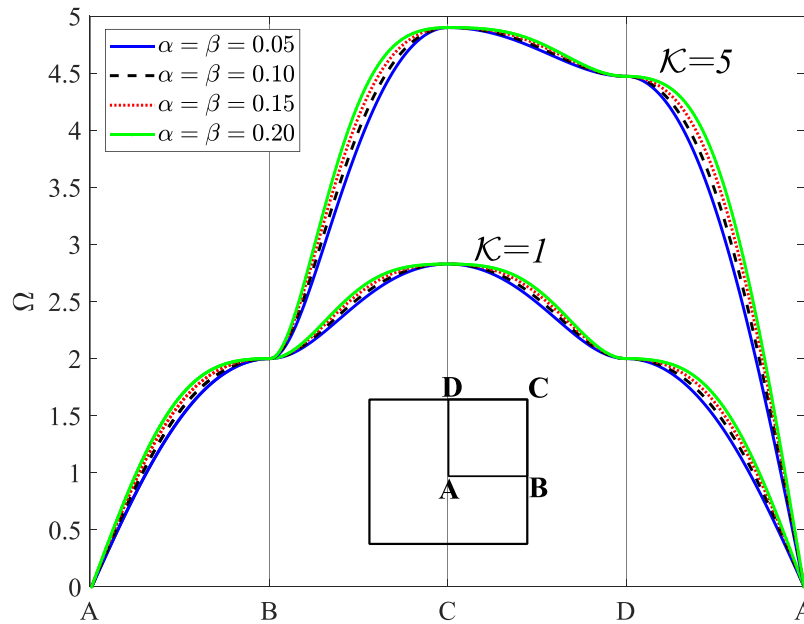


Fig. 3. Dispersion diagram of the discrete model along the edges of the IBZ. Representation of both  $\mathcal{K} = 1$  and  $\mathcal{K} = 5$  cases.

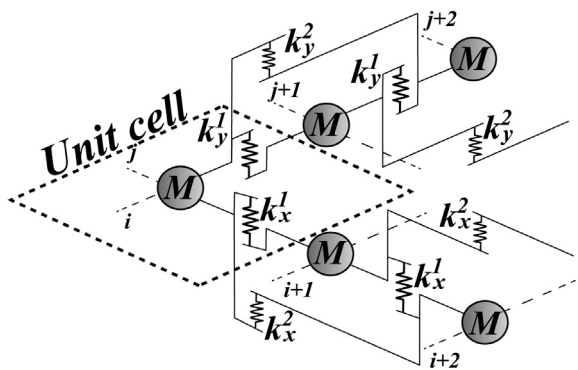


Fig. 4. Square unit cell of the lattice system.

along the axis A–B, the  $\mathcal{K} = 5$  case losing the symmetry with respect to the axis A–C, as it has been mentioned above.

### 3. Continualization procedures

Although the discrete accurately captures the size-effects, it involves a high computational cost. Therefore, the main goal of this work is to obtain non-classical continuum models, capable of reliably capturing the behaviour of the discrete one, considered as a reference. To this end, different standard and non-standard continualization methods are applied to the discrete model, as it is explained in the following sections.

#### 3.1. Standard continualization techniques

The standard continualization procedures are based on extending the discrete displacement variables by means of Taylor’s series as

$$\bar{v}_{i\pm q,j} = \bar{v} \pm \frac{\partial \bar{v}}{\partial \bar{x}} q\bar{d} + \frac{1}{2} \frac{\partial^2 \bar{v}}{\partial \bar{x}^2} (q\bar{d})^2 \pm \frac{1}{6} \frac{\partial^3 \bar{v}}{\partial \bar{x}^3} (q\bar{d})^3 + \frac{1}{24} \frac{\partial^4 \bar{v}}{\partial \bar{x}^4} (q\bar{d})^4 \pm O\left(\frac{\partial^5}{\partial \bar{x}^5}\right); \quad (9)$$

$$\bar{v}_{i,j\pm q} = \bar{v} \pm \frac{\partial \bar{v}}{\partial \bar{y}} q\bar{d} + \frac{1}{2} \frac{\partial^2 \bar{v}}{\partial \bar{y}^2} (q\bar{d})^2 \pm \frac{1}{6} \frac{\partial^3 \bar{v}}{\partial \bar{y}^3} (q\bar{d})^3 + \frac{1}{24} \frac{\partial^4 \bar{v}}{\partial \bar{y}^4} (q\bar{d})^4 \pm O\left(\frac{\partial^5}{\partial \bar{y}^5}\right),$$

(10)

where  $\bar{v}(\bar{x}, \bar{y}, \tau)$  is the continuous displacement variable such thus  $\bar{v}_{i,j}(\tau) = \bar{v}(\bar{x}_i, \bar{y}_j, \tau)$ . Note that when dimensionless variables are employed,  $\bar{d} = d/d = 1$ , so the approximation order is specified by the order of the dimensionless spatial derivative (Andrianov et al., 2010; Gómez-Silva et al., 2020).

In the following, two different standard continualization procedures will be used. On the one hand, the displacement variables of the discrete governing equation are expanded by Taylor’s series. On the other hand, these series are directly applied to the Lagrangian of the system. These two models will be denoted throughout this paper as Standard I and II models, respectively.

##### 3.1.1. Standard I model

Disregarding terms higher than second order, in both  $x$  and  $y$  directions, when Eqs. (9) and (10) are applied in Eq. (5), the following continuum governing equation is obtained

$$b_1 \frac{\partial^2 \bar{v}}{\partial \bar{x}^2} + b_2 \mathcal{K} \frac{\partial^2 \bar{v}}{\partial \bar{y}^2} = \frac{\partial^2 \bar{v}}{\partial \tau^2}, \quad (11)$$

where

$$b_1 = 1 + 4\alpha; \quad b_2 = 1 + 4\beta. \quad (12)$$

This equation is similar to the classical governing equation of anisotropic membranes, but including factors  $b_1$  and  $b_2$ , which account for long-range forces by means of the dimensionless parameters  $\alpha$  and  $\beta$ . For this reason, this model will be called as Classical model in this paper, whose dispersion relation can be found by assuming the plane wave

$$\bar{v} = V e^{i(\bar{K}_x \bar{x} + \bar{K}_y \bar{y} - \Omega \tau)}, \quad (13)$$

as a solution of Eq. (11), it leading to

$$\Omega = \sqrt{b_1 \bar{K}_x^2 + b_2 \mathcal{K} \bar{K}_y^2}, \quad (14)$$

which shows isotropic character when  $\mathcal{K} = 1$ , it being anisotropic for  $\mathcal{K} \neq 1$ , feature that applies to all the continuum models developed in this work. On the other hand, although this model successfully describes the propagation of long waves ( $\bar{K} \rightarrow 0$ ), it fails when size-effects play a role (high wavenumbers). Aiming to capture the dispersive

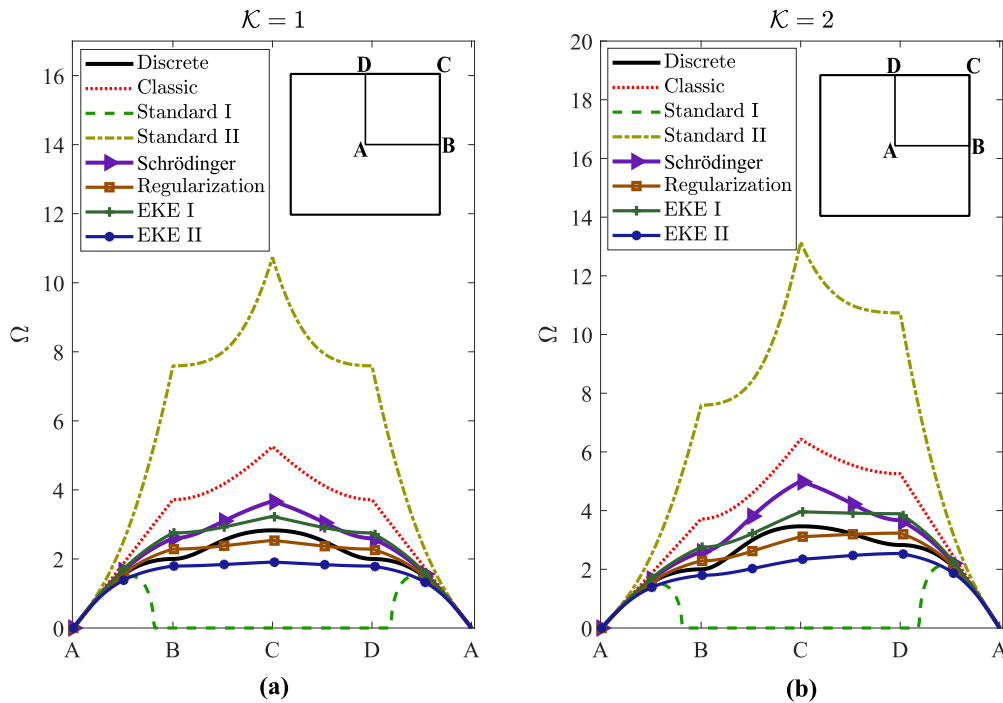


Fig. 5. Comparison of dispersion curves of the continuum models with that of the discrete one, considered as a reference. Exhibition of (a)  $\mathcal{K} = 1$  and (b)  $\mathcal{K} = 2$  cases with  $\alpha = \beta = 0.1$ .

behaviour of the discrete model with greater accuracy, terms up to the fourth order are considered when Eq. (5) is expanded, it resulting in the non-classical continuum governing equation

$$b_1 \frac{\partial^2 \bar{v}}{\partial \bar{x}^2} - a_1 \frac{\partial^4 \bar{v}}{\partial \bar{x}^4} + \mathcal{K} \left( b_2 \frac{\partial^2 \bar{v}}{\partial \bar{y}^2} - a_2 \frac{\partial^4 \bar{v}}{\partial \bar{y}^4} \right) = \frac{\partial^2 \bar{v}}{\partial \tau^2}, \quad (15)$$

where two scale parameter  $a_1$  and  $a_2$  appear

$$a_1 = -\frac{1+16\alpha}{12}; \quad a_2 = -\frac{1+16\beta}{12}. \quad (16)$$

The dispersion relation of this model reads

$$\Omega = \sqrt{b_1 \bar{K}_x^2 + a_1 \bar{K}_x^4 + \mathcal{K} (b_2 \bar{K}_y^2 + a_2 \bar{K}_y^4)}. \quad (17)$$

### 3.1.2. Standard II model

This model is developed by employing the continualization procedure that [Polyzos and Fotiadis \(2012\)](#) suggest for axial lattice systems. This continualization method consists in expanding the discrete displacement variables in the Lagrangian of the discrete model. To this end, we employed the cell displayed in [Fig. 4](#), which includes the primary springs connecting particles with indices  $(i, j)$  and  $(i, j + 1)$ , and  $(i, j)$  and  $(i + 1, j)$ , and the secondary ones linking particles with indices  $(i, j)$  and  $(i, j + 2)$ , and  $(i, j)$  and  $(i + 2, j)$ . Therefore, the discrete potential energy density reads

$$\begin{aligned} \bar{W}_s = & \frac{1}{2} \left[ (\bar{v}_{i+1,j} - \bar{v}_{i,j})^2 + \mathcal{K} (\bar{v}_{i,j+1} - \bar{v}_{i,j})^2 \right] \\ & + \frac{1}{2} \left[ \alpha (\bar{v}_{i+2,j} - \bar{v}_{i,j})^2 + \beta \mathcal{K} (\bar{v}_{i,j+2} - \bar{v}_{i,j})^2 \right], \end{aligned} \quad (18)$$

where  $\bar{W}_s = W_s / (d^2 k_x)$ ,  $W_s$  being its dimensional counterpart. Expanding Eq. (18) via Taylor's series up to second order, it yields to

$$\begin{aligned} \bar{W}_s = & \frac{1}{2} \left( \frac{\partial \bar{v}}{\partial \bar{x}} + \frac{1}{2} \frac{\partial^2 \bar{v}}{\partial \bar{x}^2} \right)^2 + \frac{\mathcal{K}}{2} \left( \frac{\partial \bar{v}}{\partial \bar{y}} + \frac{1}{2} \frac{\partial^2 \bar{v}}{\partial \bar{y}^2} \right)^2 \\ & + 2\alpha \left( \frac{\partial \bar{v}}{\partial \bar{x}} + \frac{\partial^2 \bar{v}}{\partial \bar{x}^2} \right)^2 + 2\beta \mathcal{K} \left( \frac{\partial \bar{v}}{\partial \bar{y}} + \frac{\partial^2 \bar{v}}{\partial \bar{y}^2} \right)^2. \end{aligned} \quad (19)$$

Taking into account Eq. (19), and the classical dimensionless kinetic energy density

$$\bar{T}_s = \frac{1}{2} \left( \frac{\partial \bar{v}}{\partial \tau} \right)^2, \quad (20)$$

where  $\bar{T}_s = T_s / (l^2 k_x)$ ,  $T_s$  being its dimensional counterpart, the Lagrangian of this model can be determined by

$$\bar{\mathcal{L}} = \iint_S (\bar{T}_s - \bar{W}_s) d\bar{x}d\bar{y}, \quad (21)$$

where  $S$  is the area of an equivalent continuous membrane, and  $\bar{\mathcal{L}} = \mathcal{L} / k_x$ ,  $\mathcal{L}$  is its dimensional counterpart. Therefore, applying Hamilton's Principle to Eq. (21), the next governing equation is obtained

$$b_1 \frac{\partial^2 \bar{v}}{\partial \bar{x}^2} - a_1 \frac{\partial^4 \bar{v}}{\partial \bar{x}^4} + \mathcal{K} \left( b_2 \frac{\partial^2 \bar{v}}{\partial \bar{y}^2} - a_2 \frac{\partial^4 \bar{v}}{\partial \bar{y}^4} \right) = \frac{\partial^2 \bar{v}}{\partial \tau^2}, \quad (22)$$

where

$$b_1 = 1 + 4\alpha; \quad b_2 = 1 + 4\beta; \quad a_1 = \frac{1+16\alpha}{4}; \quad a_2 = \frac{1+16\beta}{4}. \quad (23)$$

This governing equations is formally equivalent to that of the Standard I model, the only difference being in the value of the scale parameters  $a_1$  and  $a_2$ . Hence, the dispersive behaviour of this model is given by Eq. (17).

### 3.2. Non-standard continualization techniques

Now, we are going to employ non-standard continualization techniques, which are based on the use of the *shift* operator to expand the discrete displacement variables (see [Maslov \(1976\)](#), [Shubin \(1987\)](#) for more details) as follows

$$\bar{v}_{i+p,j+q} = \sum_{h=0}^{\infty} \frac{1}{h!} (p\partial_{\bar{x}} + q\partial_{\bar{y}})^h \bar{v}_{i,j} = e^{p\partial_{\bar{x}} + q\partial_{\bar{y}}} \bar{v}_{i,j}; \quad p, q \in \mathbb{Z}, \quad (24)$$

where  $\partial_{\bar{x}}$  and  $\partial_{\bar{y}}$  refer to the dimensionless spatial derivatives in  $x$  and  $y$  directions.

In this section, this pseudo-differential operator is going to be employed in four different ways. Firstly, a continualization procedure

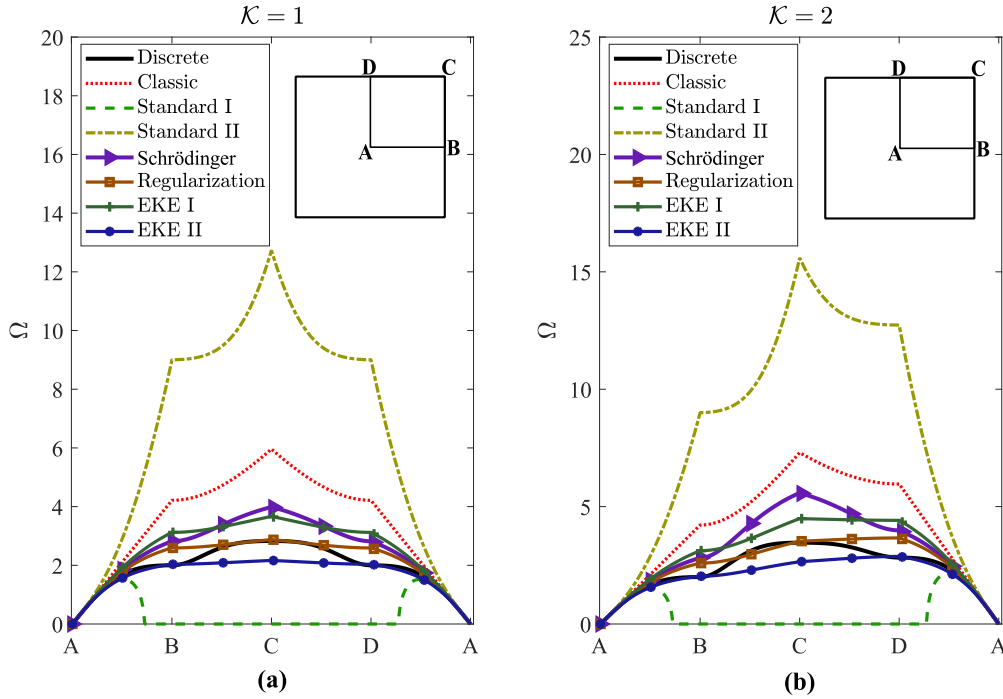


Fig. 6. Comparison of dispersion curves of the continuum models with that of the discrete one, considered as a reference. Exhibition of (a)  $\mathcal{K} = 1$  and (b)  $\mathcal{K} = 2$  cases with  $\alpha = \beta = 0.2$ .

proposed by Rosenau (1987) for a square membrane lattice only with nearest interactions is employed, which makes use of Schrödinger operators. On the other hand, the Regularization procedure, suggested by Bacigalupo and Gamarotta (2021) for a square membrane lattice with nearest interactions, and prestressed cable-net instead of linear springs, is also considered. Subsequently, the shift operator is introduced in the energy of the system, following two different approaches, thus leading to two Enriched Kinetic Energies, never before proposed for lattice systems like the one here studied. In the remainder of the paper, these models will be called as Schrödinger, Regularization, EKE I and EKE II, respectively.

### 3.3. Schrödinger model

Rosenau (1987) applied a continualization method based on Schrödinger operators to different lattice structures different from the one studied here. According to this procedure, the governing equation of the Standard I model, Eq. (15), can be rewritten by means of pseudo-differential operators as

$$P_{x1} \frac{\partial^2 \bar{v}}{\partial x^2} + P_{y1} \frac{\partial^2 \bar{v}}{\partial y^2} + 4P_{x2} \frac{\partial^2 \bar{v}}{\partial x^2} + 4P_{y2} \frac{\partial^2 \bar{v}}{\partial y^2} = \frac{\partial^2 \bar{v}}{\partial \tau^2}, \quad (25)$$

where

$$P_{x1} = 1 + \frac{\partial_x^2}{12}; \quad P_{x2} = 1 + \frac{\partial_x^2}{3}; \quad P_{y1} = 1 + \frac{\partial_y^2}{12}; \quad P_{y2} = 1 + \frac{\partial_y^2}{3}. \quad (26)$$

The above four operators are considered Schrödinger ones, and thus invertible. Since next-nearest interactions are considered in this case, two operators depending on the derivative in each  $x$ - and  $y$ -directions are involved, which can be related as suggested by Rosenau (1987) for a one-dimensional lattice with next-nearest interactions as follows

$$P_{Ax} = B_{x1} P_{x1} + B_{x2} P_{x2} = 1 + \frac{\gamma_x}{12} \partial_x; \quad (27)$$

$$P_{Ay} = B_{y1} P_{y1} + B_{y2} P_{y2} = 1 + \frac{\gamma_y}{12} \partial_y, \quad (28)$$

where

$$B_{x1} = \frac{1}{1+\alpha}; \quad B_{x2} = \frac{\alpha}{1+\alpha}; \quad B_{y1} = \frac{1}{1+\beta}; \quad B_{y2} = \frac{\beta}{1+\beta}, \quad (29)$$

and

$$\gamma_x = \frac{1+4\alpha}{1+\alpha}; \quad \gamma_y = \frac{1+4\beta}{1+\beta}. \quad (30)$$

Since both Eqs. (27) and (28) are Schrödinger operators, these can be inverted as

$$L_A^{-1} = L_{Ax}^{-1} L_{Ay}^{-1} = \left(1 - \frac{\gamma_x}{12} \partial_x\right) \left(1 - \frac{\gamma_y}{12} \partial_y\right). \quad (31)$$

Then, multiplying Eq. (25) by Eq. (31), and disregarding terms higher than fourth order, it results in

$$\begin{aligned} b_1 \frac{\partial^2 \bar{v}}{\partial x^2} + b_2 \mathcal{K} \frac{\partial^2 \bar{v}}{\partial y^2} - a_3 \frac{\partial^4 \bar{v}}{\partial x^2 \partial y^2} \\ = \frac{\partial^2 \bar{v}}{\partial \tau^2} - a_4 \frac{\partial^4 \bar{v}}{\partial x^2 \partial \tau^2} - a_5 \frac{\partial^4 \bar{v}}{\partial y^2 \partial \tau^2} + a_6 \frac{\partial^6 \bar{v}}{\partial x^2 \partial y^2 \partial \tau^2}, \end{aligned} \quad (32)$$

where

$$b_1 = 1 + 4\alpha; \quad b_2 = 1 + 4\beta; \quad (33)$$

$$a_3 = \frac{(1+4\alpha)\gamma_y}{12} + \frac{\mathcal{K}(1+4\beta)\gamma_x}{12}; \quad a_4 = \frac{\gamma_x}{12}; \quad a_5 = \frac{\gamma_y}{12}; \quad a_6 = \frac{\gamma_x \gamma_y}{144}, \quad (34)$$

size-effects being taken into account by means of the terms with spatial cross derivatives (those multiplied by  $a_3$  and  $a_6$ ) that, although formally of higher order, they do not require the use of extra boundary conditions (Rosenau, 1987). On the other hand, the terms with space-time cross derivatives increase the compliance of the model according to the dispersion relation

$$\Omega = \sqrt{\frac{b_1 \bar{K}_x^2 + b_2 \mathcal{K} \bar{K}_y^2 + a_3 \bar{K}_x^2 \bar{K}_y^2}{1 + a_4 \bar{K}_x^2 + a_5 \bar{K}_y^2 + a_6 \bar{K}_x^2 \bar{K}_y^2}}. \quad (35)$$

#### 3.3.1. Regularization model

Bacigalupo and Gamarotta (2021) propose a continualization procedure, which they apply to a square membrane lattice not considering

next-nearest interactions. This method is going to be used in this section, and is based on expressing the cross spatial derivative of the continuous displacement by means of the central difference scheme as

$$\frac{\partial^2 \bar{v}}{\partial \bar{x} \partial \bar{y}} \Big|_{\bar{x}_i, \bar{y}_j} = \partial_{\bar{x}} \partial_{\bar{y}} \bar{v} \Big|_{\bar{x}_i, \bar{y}_j} = \frac{\bar{v}_{i+1,j+1} - \bar{v}_{i-1,j+1} - \bar{v}_{i+1,j-1} + \bar{v}_{i-1,j-1}}{4d^2} = \frac{e^{\partial_{\bar{x}} + \partial_{\bar{y}}} - e^{-\partial_{\bar{x}} + \partial_{\bar{y}}} - e^{\partial_{\bar{x}} - \partial_{\bar{y}}} + e^{-\partial_{\bar{x}} - \partial_{\bar{y}}}}{4} \bar{v}_{i,j}. \quad (36)$$

From Eq. (36), and bearing in mind the Fourier transform and the properties of pseudo-differential operators (Bacigalupo and Gambarotta, 2019, 2021), we can obtain the expression

$$\bar{v}_{i,j} = \frac{4\partial_{\bar{x}}\partial_{\bar{y}}}{(e^{\partial_{\bar{x}}} - e^{-\partial_{\bar{x}}})(e^{\partial_{\bar{y}}} - e^{-\partial_{\bar{y}}})} \bar{v} \Big|_{\bar{x}_i, \bar{y}_j}, \quad (37)$$

which relates both discrete and continuous fields. On the other hand, the shift operator, Eq. (24), is applied to the discrete governing Eq. (5), it resulting in

$$\left[ (e^{\partial_{\bar{x}}} - 2 + e^{-\partial_{\bar{x}}}) + \mathcal{K}(e^{\partial_{\bar{y}}} - 2 + e^{-\partial_{\bar{y}}}) + \alpha(e^{2\partial_{\bar{x}}} - 2 + e^{-2\partial_{\bar{x}}}) + \beta\mathcal{K}(e^{2\partial_{\bar{y}}} - 2 + e^{-2\partial_{\bar{y}}}) \right] \bar{v}_{i,j} = \frac{\partial^2 \bar{v}_{i,j}}{\partial \tau^2}. \quad (38)$$

Therefore, if Eq. (37) is introduced into Eq. (38), considering again that  $\bar{v}_{i,j}(\tau) = \bar{v}(\bar{x}_i, \bar{y}_j, \tau)$ , the following continuous pseudo-differential governing equation is obtained

$$(P_1 + \mathcal{K}P_2 + \alpha P_3 + \beta\mathcal{K}P_4)\bar{v} = P_5 \frac{\partial^2 \bar{v}}{\partial \tau^2}, \quad (39)$$

where

$$P_1 = \frac{4\partial_{\bar{x}}\partial_{\bar{y}}(e^{\partial_{\bar{x}}} - 2 + e^{-\partial_{\bar{x}}})}{(e^{\partial_{\bar{x}}} - e^{-\partial_{\bar{x}}})(e^{\partial_{\bar{y}}} - e^{-\partial_{\bar{y}}})}; \quad (40)$$

$$P_2 = \frac{4\partial_{\bar{x}}\partial_{\bar{y}}(e^{\partial_{\bar{y}}} - 2 + e^{-\partial_{\bar{y}}})}{(e^{\partial_{\bar{x}}} - e^{-\partial_{\bar{x}}})(e^{\partial_{\bar{y}}} - e^{-\partial_{\bar{y}}})}; \quad (41)$$

$$P_3 = \frac{4\partial_{\bar{x}}\partial_{\bar{x}}(e^{2\partial_{\bar{x}}} - 2 + e^{-2\partial_{\bar{x}}})}{(e^{\partial_{\bar{x}}} - e^{-\partial_{\bar{x}}})(e^{\partial_{\bar{y}}} - e^{-\partial_{\bar{y}}})}; \quad (42)$$

$$P_4 = \frac{4\partial_{\bar{x}}\partial_{\bar{y}}(e^{2\partial_{\bar{y}}} - 2 + e^{-2\partial_{\bar{y}}})}{(e^{\partial_{\bar{x}}} - e^{-\partial_{\bar{x}}})(e^{\partial_{\bar{y}}} - e^{-\partial_{\bar{y}}})}; \quad (43)$$

$$P_5 = \frac{4\partial_{\bar{x}}\partial_{\bar{y}}}{(e^{\partial_{\bar{x}}} - e^{-\partial_{\bar{x}}})(e^{\partial_{\bar{y}}} - e^{-\partial_{\bar{y}}})}. \quad (44)$$

If Eqs. (40) to (44) are expanded via Taylor's series as

$$P_1 \approx \partial_{\bar{x}}^2 - \frac{1}{12}(\partial_{\bar{x}}^4 + 2\partial_{\bar{x}}^2\partial_{\bar{y}}^2); \quad (45)$$

$$P_2 \approx \partial_{\bar{y}}^2 - \frac{1}{12}(\partial_{\bar{y}}^4 + 2\partial_{\bar{x}}^2\partial_{\bar{y}}^2); \quad (46)$$

$$P_3 \approx 4\partial_{\bar{x}}^2 + \frac{2}{3}(\partial_{\bar{x}}^4 - \partial_{\bar{x}}^2\partial_{\bar{y}}^2); \quad (47)$$

$$P_4 \approx 4\partial_{\bar{y}}^2 + \frac{2}{3}(\partial_{\bar{y}}^4 - \partial_{\bar{x}}^2\partial_{\bar{y}}^2); \quad (48)$$

$$P_5 \approx 1 - \frac{1}{6}(\partial_{\bar{x}}^2 + \partial_{\bar{y}}^2) + \frac{7}{360}(\partial_{\bar{x}}^4 + \partial_{\bar{y}}^4), \quad (49)$$

and terms higher than second order are disregarded, the following continuous governing equation can be reached

$$b_1 \frac{\partial^2 \bar{v}}{\partial \bar{x}^2} + b_2 \mathcal{K} \frac{\partial^2 \bar{v}}{\partial \bar{y}^2} = \frac{\partial^2 \bar{v}}{\partial \tau^2} - a_4 \frac{\partial^4 \bar{v}}{\partial \bar{x}^2 \partial \tau^2} - a_5 \frac{\partial^4 \bar{v}}{\partial \bar{y}^2 \partial \tau^2}, \quad (50)$$

where

$$b_1 = 1 + 4\alpha; \quad b_2 = 1 + 4\beta; \quad a_4 = a_5 = \frac{1}{6}. \quad (51)$$

Note that this model neither presents high-order spatial derivatives, in this case not appearing the scale parameters  $a_3$  and  $a_6$ . The dispersion

relation of this model reads

$$\Omega = \sqrt{\frac{b_1 \bar{K}_x^2 + b_2 \mathcal{K} \bar{K}_y^2}{1 + a_4 \bar{K}_x^2 + a_5 \bar{K}_y^2}}. \quad (52)$$

### 3.3.2. Enriched kinetic energy I (EKE I) model

This model is developed by employing an enriched kinetic energy, which is obtained by following a procedure similar to that proposed by Rosenau (2003) for 1D axial lattices. This procedure consists in expressing the first spatial derivative of the continuous displacement via the progressive difference scheme

$$\frac{\partial \bar{v}}{\partial \bar{x} \bar{y}} \Big|_{\bar{x}_i, \bar{y}_j} = \partial_{\bar{x}} \partial_{\bar{y}} \bar{v} \Big|_{\bar{x}_i, \bar{y}_j} = \frac{\bar{v}_{i+1,j+1} - \bar{v}_{i+1,j} - \bar{v}_{i,j+1} + \bar{v}_{i,j}}{d^2}, \quad (53)$$

which, introducing the shift operator, Eq. (24), turns into

$$\partial_{\bar{x}} \partial_{\bar{y}} \bar{v} \Big|_{\bar{x}_i, \bar{y}_j} = (e^{\partial_{\bar{x}} + \partial_{\bar{y}}} - e^{\partial_{\bar{x}}} - e^{\partial_{\bar{y}}} + 1) \bar{v}_{i,j}. \quad (54)$$

In this way, the next relation between discrete and continuous displacement fields is achieved

$$\bar{v}_{i,j} = \frac{\partial_{\bar{x}} \partial_{\bar{y}}}{(e^{\partial_{\bar{x}}} - 1)(e^{\partial_{\bar{y}}} - 1)} \bar{v} \Big|_{\bar{x}_i, \bar{y}_j}, \quad (55)$$

which can be expanded through Taylor's series up to second order as

$$\bar{v}_{i,j} \approx \mathcal{Q}_1 \cdot \bar{v}, \quad (56)$$

where

$$\mathcal{Q}_1 = 1 - \frac{1}{2}(\partial_{\bar{x}} + \partial_{\bar{y}}) + \frac{1}{12}(\partial_{\bar{x}}^2 + \partial_{\bar{y}}^2) + \frac{1}{4}\partial_{\bar{x}}\partial_{\bar{y}}, \quad (57)$$

which leads to the following enriched kinetic energy density (see Appendix)

$$\bar{T}_s = \frac{1}{2} \left[ \left( \frac{\partial \bar{v}}{\partial \tau} \right)^2 + \frac{1}{12} \left( \left( \frac{\partial^2 \bar{v}}{\partial \bar{x} \partial \tau} \right)^2 + \left( \frac{\partial^2 \bar{v}}{\partial \bar{y} \partial \tau} \right)^2 \right) \right]. \quad (58)$$

Regarding the potential energy density, for this model we are going to employ one similar to the classic one, but accounting for next-nearest interactions. For this purpose, Eq. (18) is expanded via Taylor's series until first order, it yielding to

$$\bar{W}_s = \frac{1}{2} \left[ b_1 \left( \frac{\partial \bar{v}}{\partial \bar{x}} \right)^2 + b_2 \mathcal{K} \left( \frac{\partial \bar{v}}{\partial \bar{y}} \right)^2 \right], \quad (59)$$

which introduce next-nearest interactions by means of the parameters  $b_1$  and  $b_2$ . Applying the Hamilton's Principle to the Lagrangian of the model, defined by Eqs. (21), (58) and (59), the following continuous governing equation is obtained

$$b_1 \frac{\partial^2 \bar{v}}{\partial \bar{x}^2} + b_2 \mathcal{K} \frac{\partial^2 \bar{v}}{\partial \bar{y}^2} = \frac{\partial^2 \bar{v}}{\partial \tau^2} - a_4 \frac{\partial^4 \bar{v}}{\partial \bar{x}^2 \partial \tau^2} - a_5 \frac{\partial^4 \bar{v}}{\partial \bar{y}^2 \partial \tau^2}, \quad (60)$$

where

$$b_1 = 1 + 4\alpha; \quad b_2 = 1 + 4\beta; \quad a_4 = a_5 = \frac{1}{12}. \quad (61)$$

This governing equation is formally equivalent to that of the previous one, the only difference being the value of the scale parameter  $a_3$ , so the dispersion relation of this model can be given by Eq. (52).

### 3.3.3. Enriched kinetic energy II (EKE II) model

Now, we are going to follow a procedure similar to the previous one, in this case using the central difference scheme instead of the progressive one, thus leading to the expression given by Eq. (37). Therefore, expanding Eq. (37) through Taylor's series up to second order, it results in

$$\bar{v}_{i,j} \approx \mathcal{Q}_2 \cdot \bar{v}, \quad (62)$$

where

$$\mathcal{Q}_2 = 1 - \frac{1}{3}(\partial_{\bar{x}}^2 + \partial_{\bar{y}}^2), \quad (63)$$

**Table 1**  
Values of the parameters for the different continuum models.

	$b_1$	$b_2$	$a_1$	$a_2$	$a_3$	$a_4$	$a_5$	$a_6$
Classic	$1 + 4\alpha$	$1 + 4\beta$	0	0	0	0	0	0
Standard I	$1 + 4\alpha$	$1 + 4\beta$	$-\frac{(1+16\alpha)}{12}$	$-\frac{(1+16\beta)}{12}$	0	0	0	0
Standard II	$1 + 4\alpha$	$1 + 4\beta$	$-\frac{(1+16\alpha)}{4}$	$-\frac{(1+16\beta)}{4}$	0	0	0	0
Schrödinger	$1 + 4\alpha$	$1 + 4\beta$	0	0	$\frac{(1+4\alpha)\gamma_y}{12} + \frac{\kappa(1+4\beta)\gamma_x}{12}$	$\frac{\gamma_x}{12}$	$\frac{\gamma_y}{12}$	$\frac{\gamma_x\gamma_y}{144}$
Regularization	$1 + 4\alpha$	$1 + 4\beta$	0	0	0	1/6	1/6	0
EKE I	$1 + 4\alpha$	$1 + 4\beta$	0	0	0	1/12	1/12	0
EKE II	$1 + 4\alpha$	$1 + 4\beta$	0	0	0	1/3	1/3	0

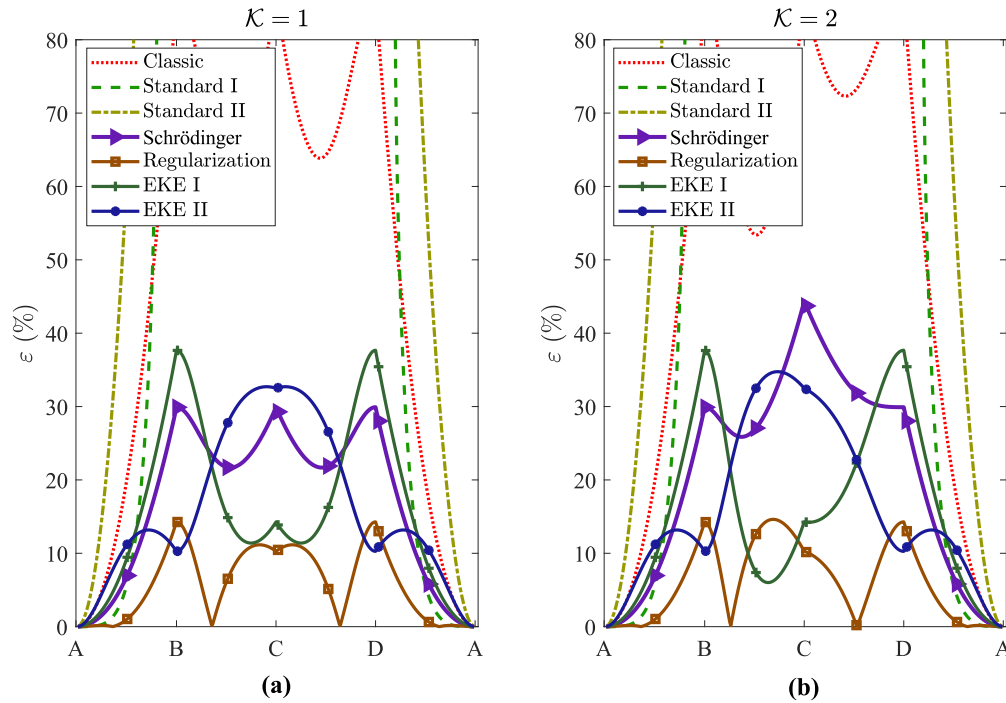


**Fig. 7.** Comparison of relative errors of the continuum models. Exhibition of (a)  $\mathcal{K} = 1$  and (b)  $\mathcal{K} = 2$  cases with  $\alpha = 0.1$ .

which leads to the following enriched kinetic energy density (see Appendix)

$$\bar{T}_s = \frac{1}{2} \left[ \left( \frac{\partial \bar{v}}{\partial \tau} \right)^2 + \frac{1}{3} \left( \left( \frac{\partial^2 \bar{v}}{\partial \bar{x} \partial \tau} \right)^2 + \left( \frac{\partial^2 \bar{v}}{\partial \bar{y} \partial \tau} \right)^2 \right) \right]. \quad (64)$$

In this case, we also consider the equivalent classical potential energy density, given by Eq. (59). Hence, applying the Hamilton's Principle to the Lagrangian of the model, Eq. (21), the next continuous governing equation is reached

$$b_1 \frac{\partial^2 \bar{v}}{\partial \bar{x}^2} + b_2 \mathcal{K} \frac{\partial^2 \bar{v}}{\partial \bar{y}^2} = \frac{\partial^2 \bar{v}}{\partial \tau^2} - a_4 \frac{\partial^4 \bar{v}}{\partial \bar{x}^2 \partial \tau^2} - a_5 \frac{\partial^4 \bar{v}}{\partial \bar{y}^2 \partial \tau^2}, \quad (65)$$

where

$$b_1 = 1 + 4\alpha; \quad b_2 = 1 + 4\beta; \quad a_4 = a_5 = \frac{1}{3}. \quad (66)$$

which is also formally equivalent to those of the two previous models, the difference lying again the value of the scale parameter  $a_3$ . Therefore, the dispersion relation of this model is defined by Eq. (52) as well.

In order to summarize all the continuum models developed in this paper, the following general governing and dispersion equations are employed

$$\begin{aligned} b_1 \frac{\partial^2 \bar{v}}{\partial \bar{x}^2} - a_1 \frac{\partial^4 \bar{v}}{\partial \bar{x}^4} + \mathcal{K} \left( b_2 \frac{\partial^2 \bar{v}}{\partial \bar{y}^2} - a_2 \frac{\partial^4 \bar{v}}{\partial \bar{y}^4} \right) - a_3 \frac{\partial^4 \bar{v}}{\partial \bar{x}^2 \partial \bar{y}^2} = \\ = \frac{\partial^2 \bar{v}}{\partial \tau^2} - a_4 \frac{\partial^4 \bar{v}}{\partial \bar{x}^2 \partial \tau^2} - a_5 \frac{\partial^4 \bar{v}}{\partial \bar{y}^2 \partial \tau^2} + a_6 \frac{\partial^6 \bar{v}}{\partial \bar{x}^2 \partial \bar{y}^2 \partial \tau^2}; \end{aligned} \quad (67)$$

$$\Omega = \sqrt{\frac{b_1 \bar{K}_x^2 + a_1 \bar{K}_x^4 + \mathcal{K} (b_2 \bar{K}_y^2 + a_2 \bar{K}_y^4) + a_3 \bar{K}_x^2 \bar{K}_y^2}{1 + a_4 \bar{K}_x^2 + a_5 \bar{K}_y^2 + a_6 \bar{K}_x^2 \bar{K}_y^2}}, \quad (68)$$

which depend on the parameters  $b_1, b_2, a_1, a_2, a_3, a_4, a_5$  and  $a_6$ , whose values are presented for each continuum model in Table 1.

#### 4. Solution for fixed-edge boundary conditions

In this section the influence of the boundary conditions on both discrete and continuum models will be studied. For this purpose, a frequency analysis is carried out, in which the most common problem of membranes is studied, which is the configuration in which all their edges are *fixed*. In this study only the non-standard models will be addressed, since the rest need extra boundary conditions to be imposed, whose physical meaning is unclear.

##### 4.1. Continuum models

Although the model here considered do not require extra boundary conditions, they introduce non-classical parameters, so the boundary conditions needed to solve them may differ from the classical ones. To know the corresponding boundary conditions, we propose an axiomatic model, which is based on the potential energy

$$\bar{W}_s = \frac{1}{2} \left[ b_1 \left( \frac{\partial \bar{v}}{\partial \bar{x}} \right)^2 + b_2 \mathcal{K} \left( \frac{\partial \bar{v}}{\partial \bar{y}} \right)^2 + a_3 \left( \frac{\partial^2 \bar{v}}{\partial \bar{x} \partial \bar{y}} \right)^2 \right], \quad (69)$$

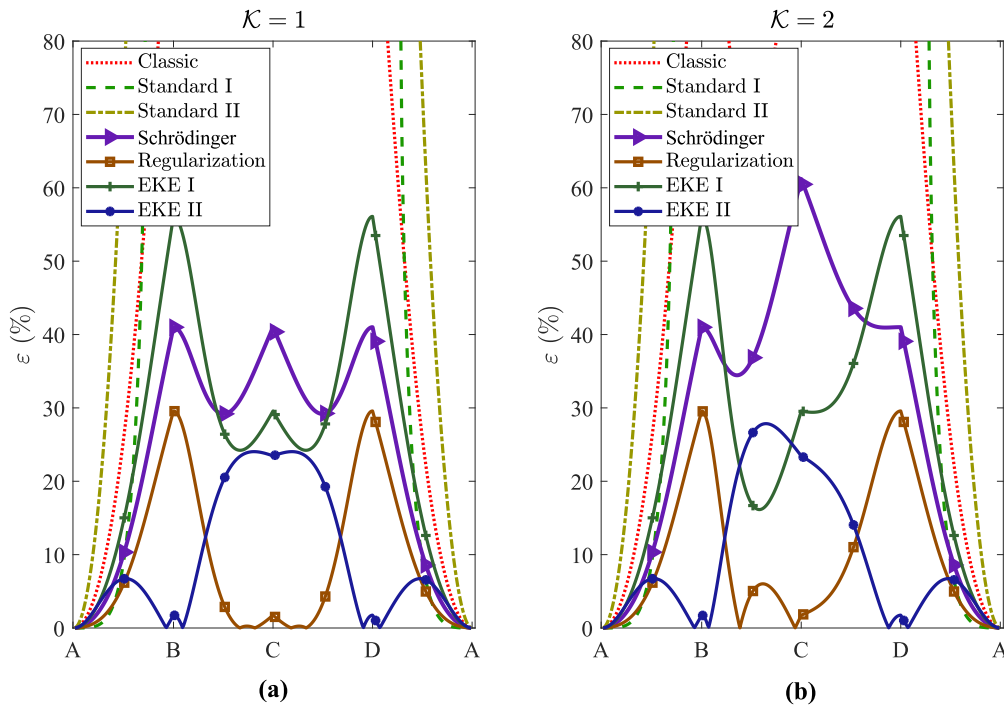


Fig. 8. Comparison of relative errors of the continuum models. Exhibition of (a)  $\mathcal{K} = 1$  and (b)  $\mathcal{K} = 2$  cases with  $\alpha = 0.2$ .

and the kinetic one

$$\bar{T}_s = \frac{1}{2} \left[ \left( \frac{\partial \bar{v}}{\partial \tau} \right)^2 + a_4 \left( \frac{\partial^2 \bar{v}}{\partial \bar{x} \partial \tau} \right)^2 + a_5 \left( \frac{\partial^2 \bar{v}}{\partial \bar{y} \partial \tau} \right)^2 + a_6 \left( \frac{\partial^3 \bar{v}}{\partial \bar{x} \bar{y} \partial \tau} \right)^2 \right]. \quad (70)$$

So, applying the Hamilton's Principle to the Lagrangian of the axiomatic model, defined by Eqs. (21), (69) and (70), the following governing equation is reached

$$b_1 \frac{\partial^2 \bar{v}}{\partial \bar{x}^2} + \mathcal{K} b_2 \frac{\partial^2 \bar{v}}{\partial \bar{y}^2} - a_3 \frac{\partial^4 \bar{v}}{\partial \bar{x}^2 \partial \bar{y}^2} = \frac{\partial^2 \bar{v}}{\partial \tau^2} - a_4 \frac{\partial^4 \bar{v}}{\partial \bar{x}^2 \partial \tau^2} - a_5 \frac{\partial^4 \bar{v}}{\partial \bar{y}^2 \partial \tau^2} + a_6 \frac{\partial^6 \bar{v}}{\partial \bar{x}^2 \partial \bar{y}^2 \partial \tau^2}, \quad (71)$$

which is formally equivalent to those of the non-standard models. On the other hand, the Hamilton's Principle also provides the corresponding boundary conditions

$$\bar{v} = 0 \quad \text{at} \quad \partial S; \quad (72)$$

or

$$\begin{aligned} & \left( b_1 \frac{\partial \bar{v}}{\partial \bar{x}} - \frac{1}{2} \left( a_3 \frac{\partial^3 \bar{v}}{\partial \bar{x} \partial \bar{y}^2} + a_6 \frac{\partial^5 \bar{v}}{\partial \bar{x} \partial \bar{y}^2 \partial \tau^2} \right) + a_4 \frac{\partial^3 \bar{v}}{\partial \bar{x} \partial \tau^2} \right) \cdot n_{\bar{x}} \\ & + \left( b_2 \mathcal{K} \frac{\partial \bar{v}}{\partial \bar{y}} - \frac{1}{2} \left( a_3 \frac{\partial^3 \bar{v}}{\partial \bar{x}^2 \partial \bar{y}} + a_6 \frac{\partial^5 \bar{v}}{\partial \bar{x}^2 \partial \bar{y} \partial \tau^2} \right) + a_5 \frac{\partial^3 \bar{v}}{\partial \bar{y} \partial \tau^2} \right) \cdot n_{\bar{y}} = 0 \quad \text{at} \quad \partial S, \end{aligned} \quad (73)$$

where  $S$  is the edge domain,  $n_{\bar{x}}$  and  $n_{\bar{y}}$  being the components of its normal vector. Applying separation of variables such that  $\bar{v}(\bar{x}, \bar{y}, \tau) = X(\bar{x})Y(\bar{y})e^{i\Omega\tau}$  is assumed as a solution of Eq. (71), it results in

$$b_1 X_{\bar{x}\bar{x}} Y + b_2 \mathcal{K} X Y_{\bar{y}\bar{y}} - a_3 X_{\bar{x}\bar{x}} Y_{\bar{y}\bar{y}} + \Omega^2 X Y - a_4 \Omega^2 X_{\bar{x}\bar{x}} Y - a_5 \Omega^2 X Y_{\bar{y}\bar{y}} + a_6 \Omega^2 X_{\bar{x}\bar{x}} Y_{\bar{y}\bar{y}} = 0, \quad (74)$$

where the subscripts  $O_{\bar{x}}$  and  $O_{\bar{y}}$  refer to the spatial derivatives in  $\bar{x}$  and  $\bar{y}$  directions, respectively. Rewriting Eq. (74) as

$$\frac{X_{\bar{x}\bar{x}}}{X} = - \left( \frac{(b_2 \mathcal{K} - a_5 \Omega^2) \frac{Y_{\bar{y}\bar{y}}}{Y} - \Omega^2}{b_1 - a_4 \Omega^2 - (a_3 - a_6 \Omega^2)} \right) = -\eta^2, \quad (75)$$

and

$$\frac{Y_{\bar{y}\bar{y}}}{Y} = - \left( \frac{(b_1 - a_4 \Omega^2) \frac{X_{\bar{x}\bar{x}}}{X} - \Omega^2}{b_2 \mathcal{K} - a_5 \Omega^2 - (a_3 - a_6 \Omega^2)} \right) = -\gamma^2, \quad (76)$$

the next spatial solutions can be found

$$X(\bar{x}) = A_1 \cos(\eta \bar{x}) + A_2 \sin(\eta \bar{x}); \quad (77)$$

$$Y(\bar{y}) = B_1 \cos(\gamma \bar{y}) + B_2 \sin(\gamma \bar{y}). \quad (78)$$

Introducing now the solution  $\bar{v}(\bar{x}, \bar{y}, \tau) = X(\bar{x})Y(\bar{y})e^{i\Omega\tau}$  in Eqs. (72) and (73), the boundary conditions read

$$X(\bar{x})Y(\bar{y}) = 0; \quad (79)$$

or

$$\begin{aligned} & \left( b_1 X_{\bar{x}}(\bar{x})Y(\bar{y}) - \frac{1}{2} \left( (a_3 - a_6 \Omega^2) X_{\bar{x}\bar{x}}(\bar{x})Y_{\bar{y}\bar{y}}(\bar{y}) - a_4 \Omega X_{\bar{x}\bar{x}}(\bar{x})Y(\bar{y}) \right) \right) \cdot n_{\bar{x}} \\ & + \left( b_2 \mathcal{K} X(\bar{x})Y_{\bar{y}}(\bar{y}) - \frac{1}{2} \left( (a_3 - a_6 \Omega^2) X_{\bar{x}\bar{x}}(\bar{x})Y_{\bar{y}}(\bar{y}) - a_5 \Omega X(\bar{x})Y_{\bar{y}}(\bar{y}) \right) \right) \cdot n_{\bar{y}} = 0, \end{aligned} \quad (80)$$

the natural one, Eq. (80), differing from that of the classical model, unless  $a_3 = a_4 = a_5 = a_6 = 0$ . In this work, we are going to solve the fixed-edge problem, so the next boundary conditions are imposed

$$X(0) = X(N_x) = Y(0) = Y(N_y) = 0. \quad (81)$$

Implementing the four boundary conditions given by Eq. (81) in Eqs. (77) and (78), it results in  $A_1 = B_1 = 0$  and

$$\eta = \frac{m\pi}{N_x}; \quad m = 1, 2, \dots \quad (82)$$

$$\gamma = \frac{n\pi}{N_y}; \quad n = 1, 2, \dots \quad (83)$$

Consequently, from Eq. (74), and bearing in mind Eqs. (75), (76), (82) and (83), the following expression can be found

$$\Omega_{m,n} = \frac{\pi}{N_x} \sqrt{(b_1 - a_3 \Omega^2) m^2 + (b_2 \mathcal{K} - a_3 \Omega^2) \frac{n^2}{\mathcal{N}^2} + (a_5 - a_6 \Omega^2) \frac{n^2 m^2}{\mathcal{N}^2 N_x^2}},$$

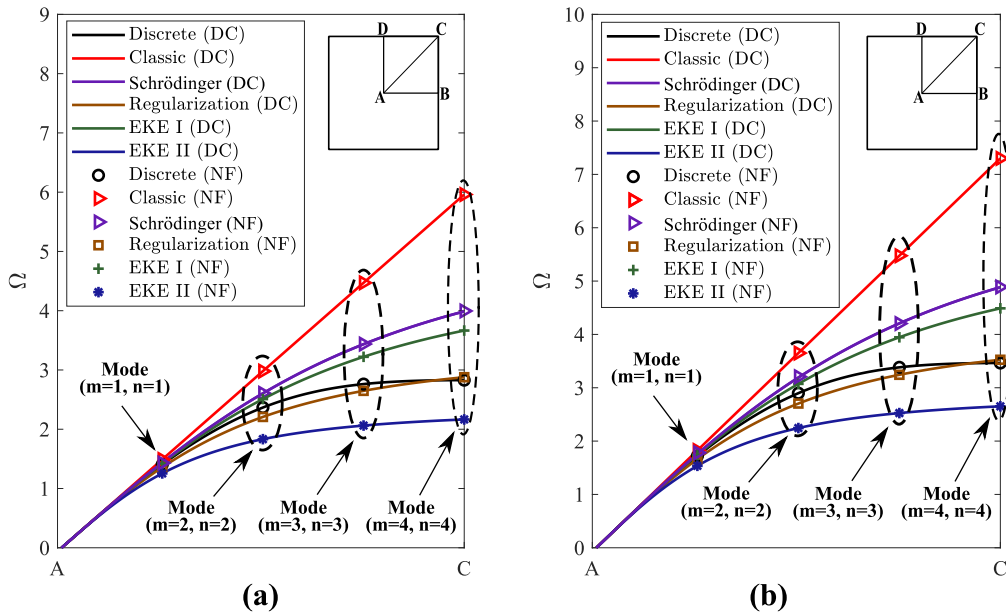


Fig. 9. Correlation between dispersion curves (DC) and natural frequencies (NF) of the square fixed-edge membrane. Comparison of the discrete model with the non-standard and Classic continuum ones, considering  $N_x = 4$ , and  $\mathcal{K} = 1$  (a) or  $\mathcal{K} = 2$  (b).

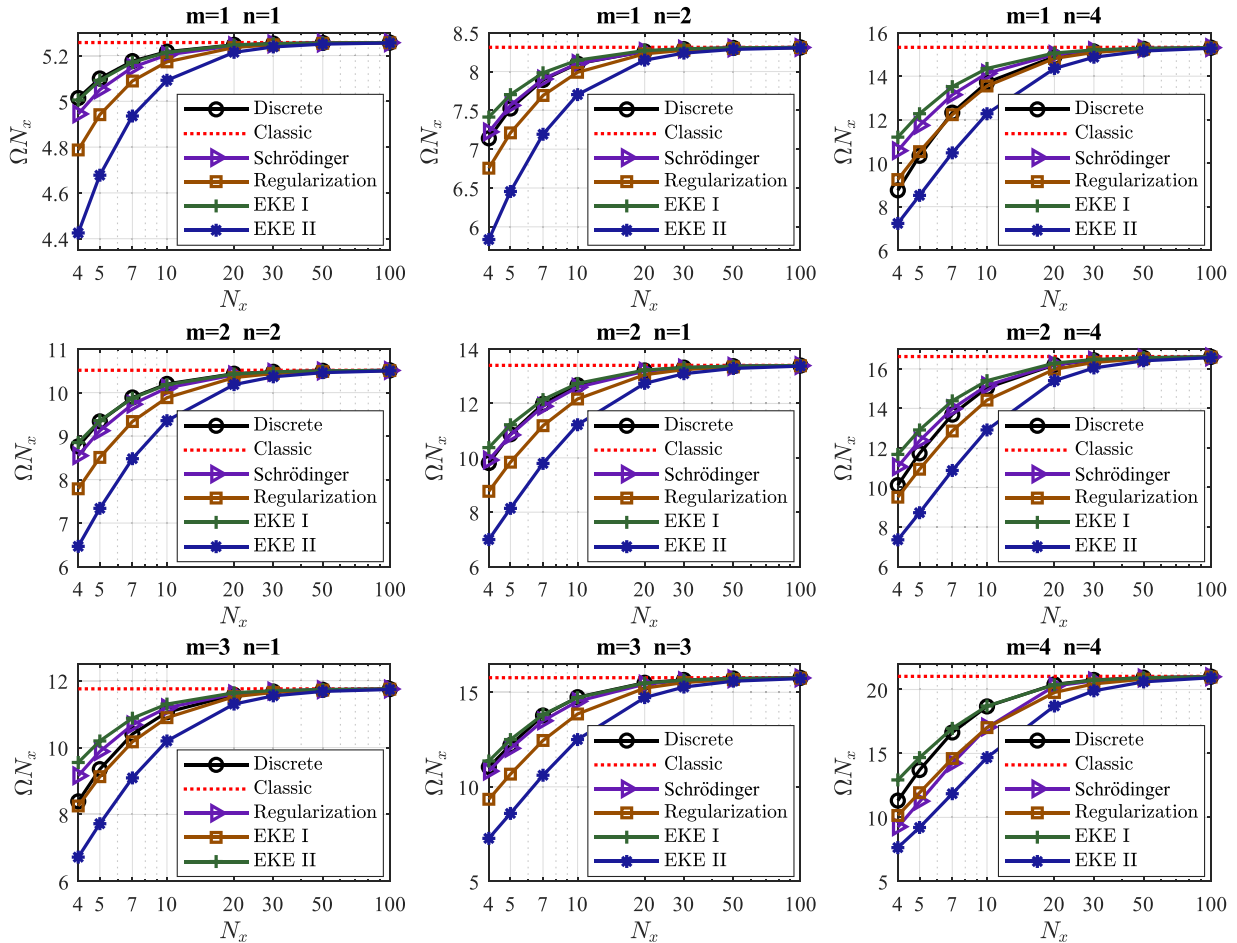


Fig. 10. Dimensionless natural frequencies of a square ( $\mathcal{N} = 1$ ) membrane with  $\mathcal{K} = 1$  for fixed-edge configuration and  $\alpha = \beta = 0.1$ . Representation of continuum and discrete models as a function of  $N_x$ .

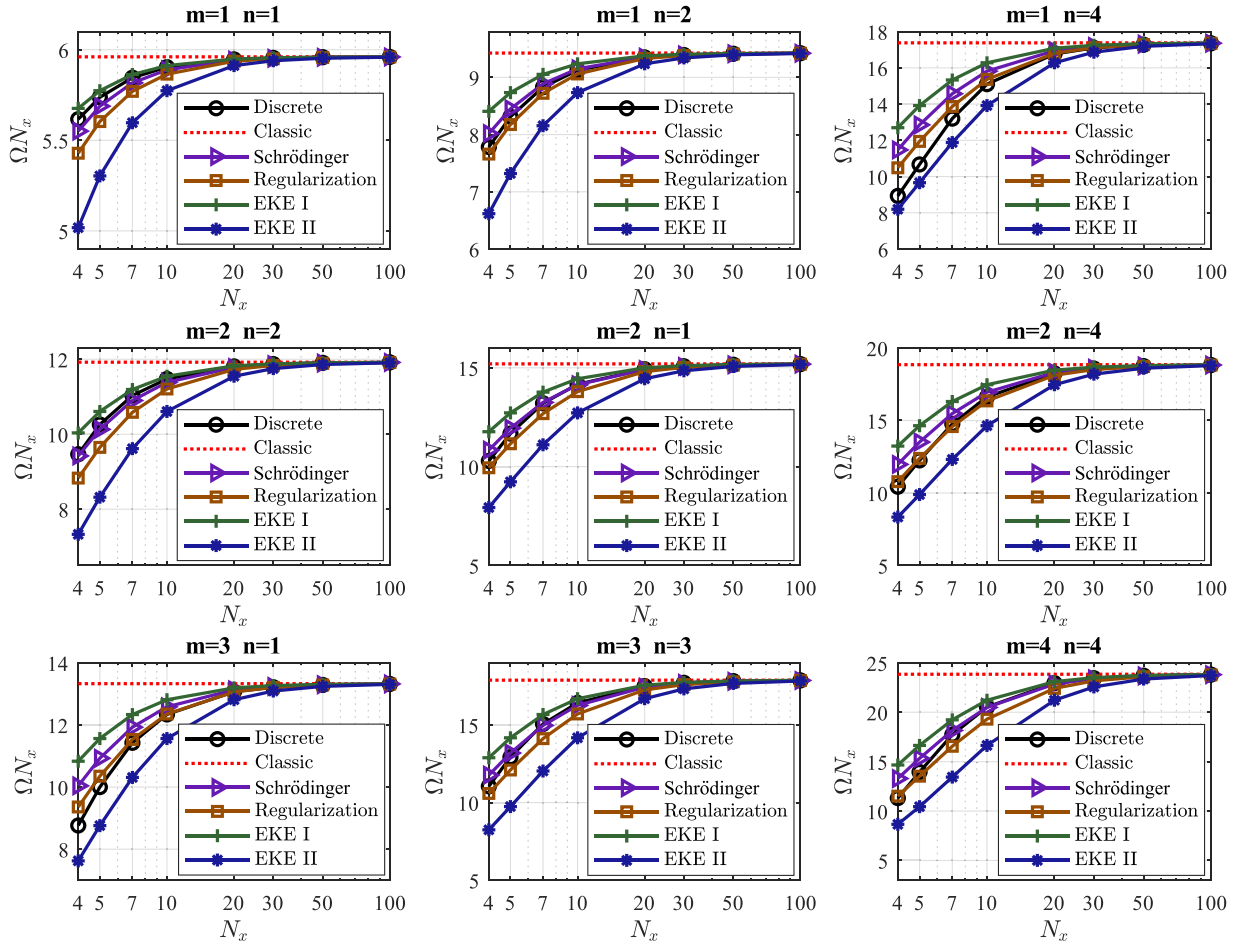


Fig. 11. Dimensionless natural frequencies of a square ( $\mathcal{N} = 1$ ) membrane with  $\mathcal{K} = 1$  for fixed-edge configuration and  $\alpha = \beta = 0.2$ . Representation of continuum and discrete models as a function of  $N_x$ .

$$(84)$$

which provides the dimensionless frequencies of the continuum models for modes  $(m, n)$ ,  $\mathcal{N} = L_y/L_x = (N_y+1)/(N_x+1)$  being the ratio between the number of particles in  $x$  and  $y$  directions. On the other hand, the corresponding vibration shape (considering unit amplitude) reads

$$\bar{v}(\bar{x}, \bar{y}) = \sin(\eta\bar{x}) \sin(\gamma\bar{y}). \quad (85)$$

#### 4.2. Discrete model

In the case of the discrete model, the natural frequencies can be found as follows. If  $\bar{v}_{i,j}(\tau) = \bar{v}_{i,j}e^{i\Omega\tau}$  is considered as a displacement solution of Eq. (5), it results in

$$\begin{aligned} & (\bar{v}_{i+1,j} - 2\bar{v}_{i,j} + \bar{v}_{i-1,j}) + \mathcal{K}(\bar{v}_{i,j+1} - 2\bar{v}_{i,j} + \bar{v}_{i,j-1}) \\ & + \alpha(\bar{v}_{i+2,j} - 2\bar{v}_{i,j} + \bar{v}_{i-2,j}) + \beta\mathcal{K}(\bar{v}_{i,j+2} - 2\bar{v}_{i,j} + \bar{v}_{i,j-2}) + \Omega^2\bar{v}_{i,j} = 0. \end{aligned} \quad (86)$$

Taking into account the vibration shape of the *fixed-edge* continuum configuration, Eq. (85), the following Ansatz of  $\bar{v}_{i,j}$  can be assumed

$$\bar{v}_{i,j} = U_o \sin\left(\frac{m\pi i}{N_x}\right) \sin\left(\frac{n\pi j}{N_y}\right); \quad m = 1, 2, \dots, N_x; \quad n = 1, 2, \dots, N_y, \quad (87)$$

as Hérissou et al. (2018) propose for a square isotopic membrane lattice without next-nearest interactions. Introducing Eq. (87) into Eq. (86),

the following expression, providing the natural frequencies of the discrete model for modes  $(m, n)$ , is reached

$$\begin{aligned} \Omega_{m,n} = & \left[ \left( 2 - 2 \cos\left(\frac{m\pi}{N_x}\right) \right) + \mathcal{K} \left( 2 - 2 \cos\left(\frac{n\pi}{\mathcal{N}N_x}\right) \right) \right. \\ & \left. + \alpha \left( 2 - 2 \cos\left(\frac{2m\pi}{N_x}\right) \right) + \beta\mathcal{K} \left( 2 - 2 \cos\left(\frac{2n\pi}{\mathcal{N}N_x}\right) \right) \right]^{\frac{1}{2}}; \end{aligned} \quad (88)$$

$$m = 1, 2, \dots, N_x; \quad n = 1, 2, \dots, N_y.$$

Note that expressions of natural frequencies for both discrete and continuum models, depend on the parameters  $\mathcal{K}$  and  $\mathcal{N}$ , which account for the anisotropy and the geometry of the rectangular lattice.

#### 5. Discussion of results

In this section, the capability of the new continuum models to capture the behaviour of the discrete one is going to be evaluated in two different ways. Firstly, their dispersion curves will be compared to that of the discrete model, subsequently, relating these curves with the natural frequencies. Finally, a natural frequency analysis will be conducted by following the procedure explained in Section 4. In order to provide more insight into both analyses, the relative errors of the continuum models will be presented, which are given by

$$\varepsilon(\%) = \frac{|\Omega_{\text{continuum}} - \Omega_{\text{discrete}}|}{\Omega_{\text{discrete}}} \times 100. \quad (89)$$

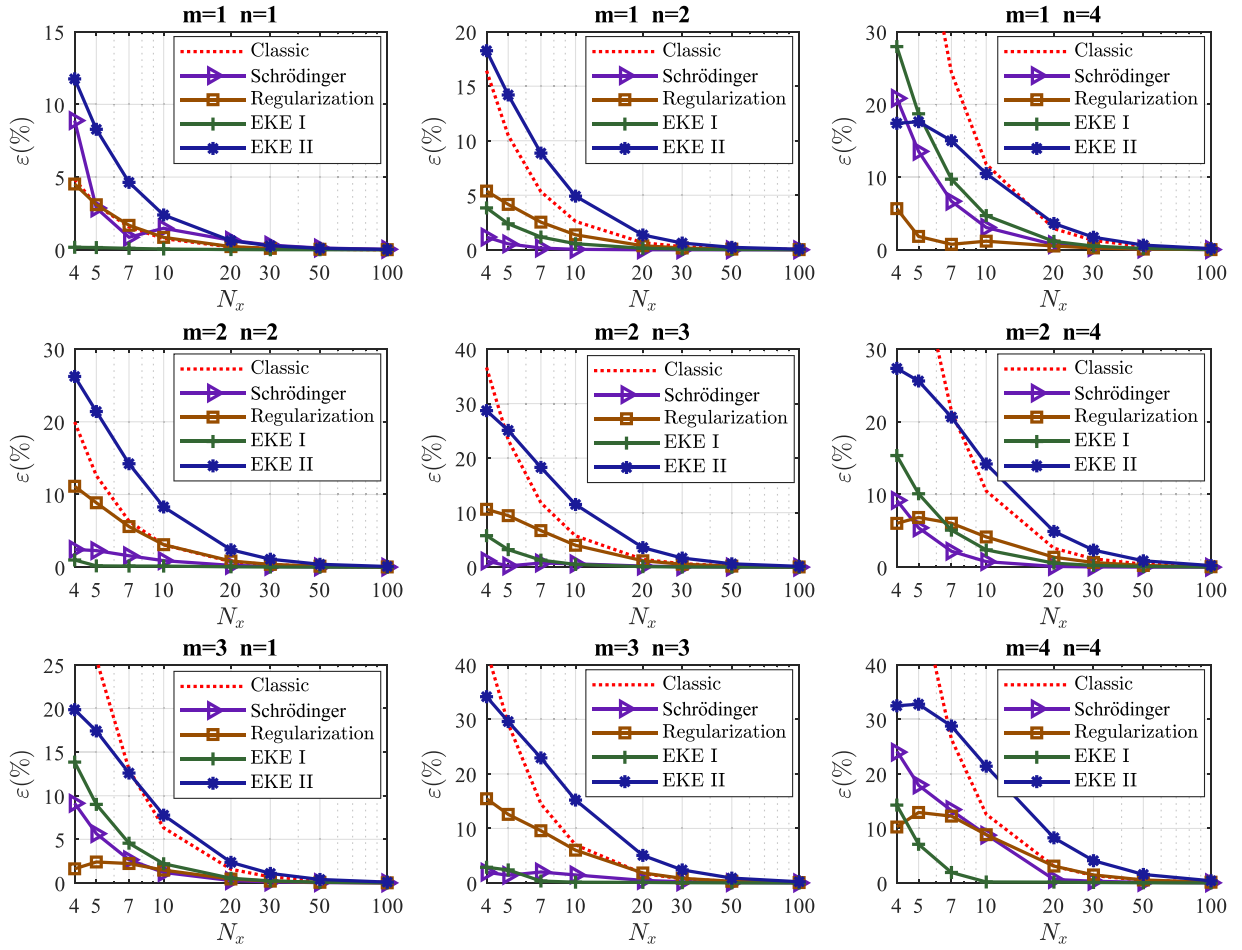


Fig. 12. Relative errors of a square ( $\mathcal{N} = 1$ ) membrane with  $\mathcal{K} = 1$  for fixed-edge configuration and  $\alpha = \beta = 0.1$ . Comparison between continuum models as a function of  $N_x$ .

### 5.1. Dispersion analysis

The dispersion curves of the continuum models along the edges of the IBZ (defined in Section 2), together with that of the discrete one, are displayed in Figs. 5 and 6 for  $\alpha = \beta = 0.1$  and  $\alpha = \beta = 0.2$ , respectively. In these figures, two different solids, one with  $\mathcal{K} = 1$  (a) and  $\mathcal{K} = 2$  (b), are considered. As it can be seen, the dispersion of all the continuum models match around vertex A of the IBZ (low wavenumber range), accurately reflecting the behaviour of the discrete one, irrespective of the value of  $\mathcal{K}$ . Nevertheless, it does not occur for higher wavenumber ranges (size-effects play a role), where each model shows different behaviour, which change with the value of  $\mathcal{K}$ .

Analysing the performance of the continuum models, it can be observed that the Standard I model shows imaginary frequencies for certain wavenumbers. This means that short waves grow exponentially in time, which does not make sense in a conservative system without any external energy source (see [Metrikine and Askes \(2002\)](#) for more details on this matter for a 1D rod lattice). Another physical feature that is worth assessing is whether the new continuum models present a maximum velocity at which disturbances can be propagated ([Metrikine and Askes, 2002](#); [Gómez-Silva and Zaera, 2022](#)). To this end, the modulus of the group velocity of the continuum model

$$|\bar{v}_g| = \sqrt{\left(\frac{\partial \Omega}{\partial \bar{K}_x}\right)^2 + \left(\frac{\partial \Omega}{\partial \bar{K}_y}\right)^2}, \quad (90)$$

where  $\bar{K}_x = |\bar{K}| \cos(\theta)$  and  $\bar{K}_y = |\bar{K}| \sin(\theta)$ ,  $\theta$  being the angle that define the direction of wave propagation, has been tested in the short-wavelength limit. Therefore, after evaluating Eq. (90) when  $|\bar{K}| \rightarrow \infty$ ,

it has been verified that the group velocity of the Standard models is unbounded for any value of  $\alpha$ . This does not occur in the non-standard models, which include the scale parameter  $a_3$ , increasing their compliance.

Now, the continuum models are assessed more closely by means of their relative error curves, presented in Figs. 7 and 8 for  $\alpha = \beta = 0.1$  and  $\alpha = \beta = 0.2$ , respectively, accounting for both  $\mathcal{K} = 1$  and  $\mathcal{K} = 2$  cases. In Fig. 7, it can be seen how the Regularization model is the one that shows the best performance for  $\mathcal{K} = 1$ , the EKE II model presenting the lowest error at vertices B and D of the IBZ. For  $\mathcal{K} = 2$ , both models exhibit a similar behaviour, the EKE I model lowering its error for high values of  $\bar{K}_x$  and  $\bar{K}_y$  (around vertex C of the IBZ). On the other hand, Fig. 8 shows how, when long-range interactions become more relevant ( $\alpha = 0.2$ ), the Regularization model shows very low errors around the vertex C of the IBZ, it increasing at vertex B and D, where the EKE II model is the one that best captures the behaviour of the discrete model. These performances appear in both  $\mathcal{K} = 1$  and  $\mathcal{K} = 2$  cases. Note that the EKE I model again decreases its error around the vertex C for  $\mathcal{K} = 2$ , but in this case it being higher than for  $\alpha = 0.1$ . As it can be seen, the Schrödinger model behaves in a similar way to the EKE I model (both  $\alpha = 0.1$  and  $\alpha = 0.2$ ), except around the limit of the IBZ, where the error of the former increases, while that of the latter decreases. Moreover, the Schrödinger model worsens its behaviour when  $\mathcal{K} = 2$ .

### 5.2. Correlation between dispersion relation and eigenpairs

In this section, the dispersion curves along the line A-C of the IBZ are going to be related to the vibrational response of the bounded solids, with the aim of completing the comparison of the behaviour of the

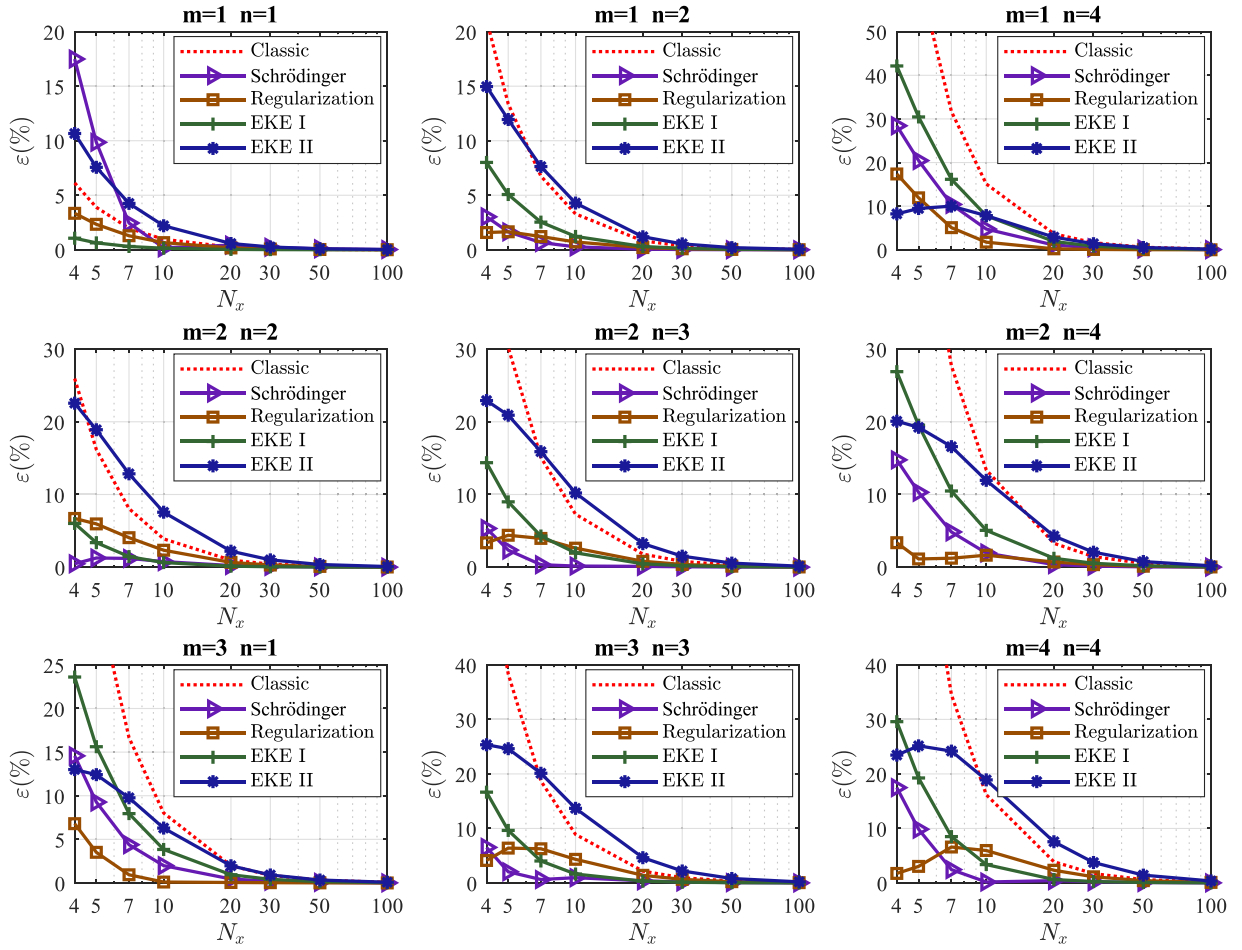


Fig. 13. Relative errors of a square ( $\mathcal{N} = 1$ ) membrane with  $\mathcal{K} = 1$  for fixed-edge configuration and  $\alpha = \beta = 0.2$ . Comparison between continuum models as a function of  $N_x$ .

models along the line A-C of the IBZ (not previously studied), as well as validating the edge treatment carried out in Section 4.

As it has been described in Section 4, the mode shapes of both discrete and continuum models are defined by harmonic functions (Eqs. (85) and (87), respectively). For this reason, the eigenpairs of the bounded solids can be related to the dispersion curves for each model. In Gómez-Silva and Zaera (2022) an exhaustive discussion about this matter can be found, where it is shown how the mode shapes  $\bar{v}_{m,n}$ , with  $m = n$ , which are characterized by *stationary* waves with vibration frequency  $\Omega_{m,n}$ , can be produced by the superposition of four *travelling* waves of the same wavenumber propagating in different directions. Hence, the dispersion curves along the line A-C of the IBZ can be related with the natural frequencies of modes described by Eq. (85), with  $m = n$ , the corresponding wavenumbers being given by

$$\bar{K}_x = \bar{K}_y = \frac{\pi m}{N_x}. \quad (91)$$

Fig. 9 shows both the dispersion relation along the line A and C of the IBZ, and the natural frequencies obtained for the fixed-edge configuration, considering  $N_x = 4$  and  $\mathcal{K} = 1$  (a) or  $\mathcal{K} = 2$  (b). It can be seen how the modes with  $m = n$  match accurately with the dispersion curves, the mode  $m = n = N_x$  corresponding to the vertex C of the IBZ, which supports the validity of the edge treatment carried out in Section 4. Moreover, it means that the trend of the dispersion relation along the line A-C can be described by the corresponding natural frequencies for the modes  $m = n = 1, \dots, N_x$ . On the other hand, it can be proven how the destructive interference of the four travelling waves causes null amplitude at the mass positions for the discrete system when  $m = n = N_x$  (see Eq. (87)). Nonetheless, the

natural frequencies corresponding to these modes ( $m = n = N_x$ ) refer to the frequency at which a travelling wave with  $\bar{K}_x = \bar{K}_y = \pi$  is propagated.

### 5.3. Natural frequencies

Now, we are going to carry out a natural frequency analysis for the fixed-edge configuration, following the procedures given in Section 4. As illustrative examples, two different membranes will be studied, one being square ( $\mathcal{N} = 1$ ) with  $\mathcal{K} = 1$ , and the other one being rectangular with  $\mathcal{N} = 2$  and  $\mathcal{K} = 2$ . Moreover, the influence of the long-range interactions is going to be analysed, taking  $\alpha = 0.1$  and  $\alpha = 0.2$ , and considering that  $\beta = \alpha$ . Several vibration modes will be showed, presenting their dimensional natural frequencies as a function of  $N_x$ , considering  $\sqrt{\mathcal{N}T_x/(\rho L_x L_y)} = 1$  (see Gómez-Silva and Zaera (2022) for more details).

#### 5.3.1. Square membrane with $\mathcal{K} = 1$

Figs. 10 and 11 show the dimensional natural frequencies of two square ( $\mathcal{N} = 1$ ) membranes with  $\mathcal{K} = 1$ , considering  $\alpha = 0.1$  and  $\alpha = 0.2$ , respectively. Note that in this case, double eigenvalues arise, corresponding to the modes  $(m, n)$  and  $(n, m)$ , with  $n \neq m$ ,  $m = 1, \dots, N_x$ ;  $n = 1, \dots, N_y$ . In both figures, it can be seen how all models converge to the same frequency when  $N_x$  increases, the value of this frequency coinciding with that of the Classic model, which is length-scale free. The reason of this performance is due to the fact that as the value of  $N_x$  grows (it means that  $N_y$  also increases for a constant value of  $\mathcal{N}$ ), the characteristic length  $d = L_x/N_x = L_y/N_y$  becomes smaller, and hence less significant when it is compared to the wavelength, thus losing

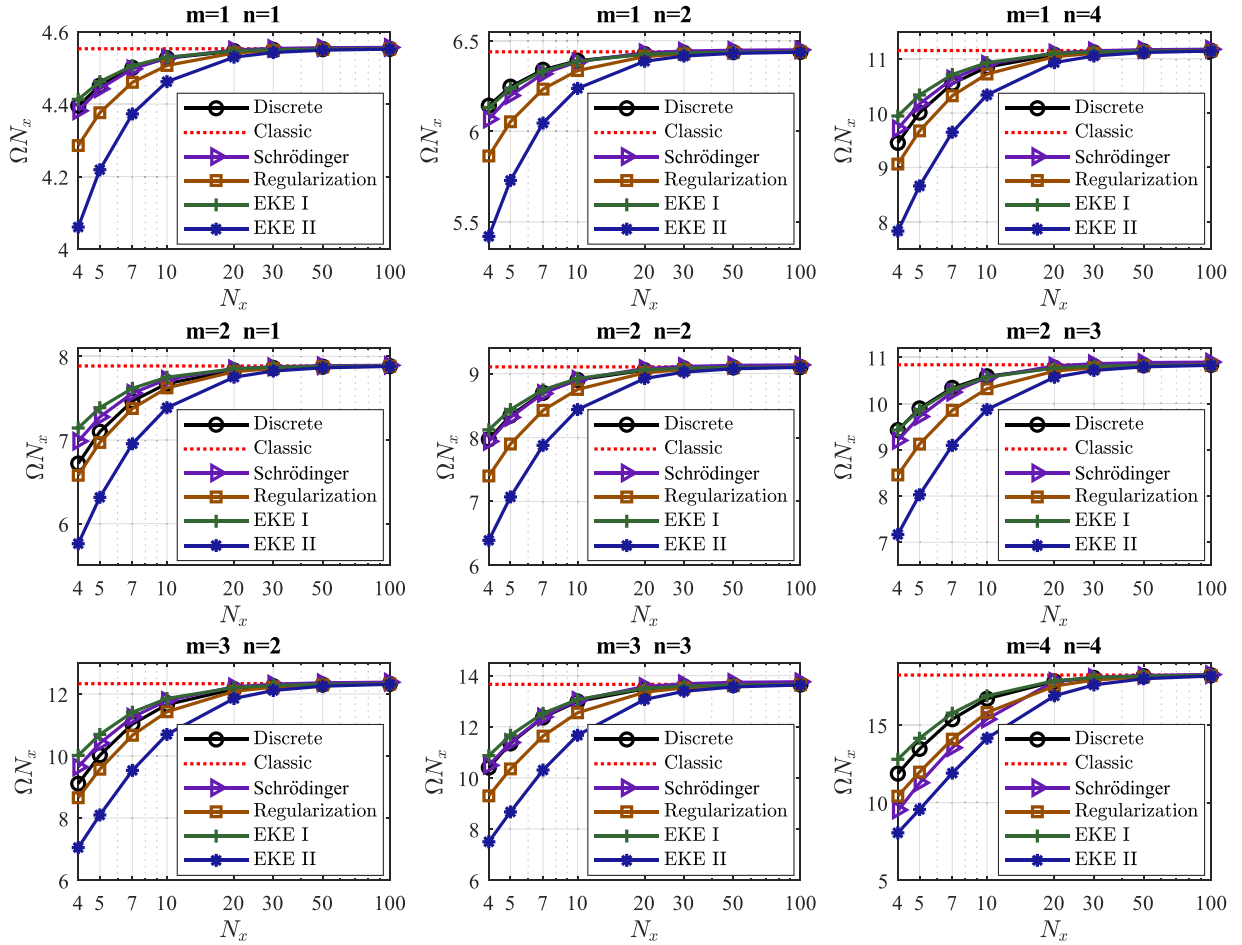


Fig. 14. Dimensionless natural frequencies of a rectangular ( $\mathcal{N} = 2$ ) membrane with  $\mathcal{K} = 2$  for fixed-edge configuration and  $\alpha = \beta = 0.1$ . Representation of continuum and discrete models as a function of  $N_x$ .

the length scale dependence. However, when  $N_x$  presents low values (length scale becomes significant), each non-classical continuum model behaves differently, capturing the size-effects with different accuracy. In order to analyse this accuracy more precisely, the relative errors of the continuum models, Eq. (89), are showed in Figs. 12 and 13 for  $\alpha = 0.1$  and  $\alpha = 0.2$ , respectively. In Fig. 12 it can be observed that for  $\alpha = 0.1$ , the Schrödinger, Regularization and EKE I models are the ones that show the best performance, with the exception of the mode ( $m = 1, n = 4$ ) (around vertices B and D of the IBZ for the square domain and  $N_x = 4$ ), where the error of the EKE I model is larger than that of the Schrödinger and EKE II model. Moreover, it can be seen how the Regularization model shows the lowest errors at the limit of the IBZ ( $N_x = 4$  and  $m$  or  $n$  equal to 4). On the other hand, when next-nearest interactions becomes more relevant ( $\alpha = 0.2$ ), it can be appreciated how the errors of the Regularization and EKE II models decrease, whereas the errors of the Schrödinger and EKE I models increase, being the Regularization model the one that shows the best performance in this case, with the exception of the mode ( $m = 1, n = 4$ ), where the EKE II model exhibits the lowest error at the limit of the IBZ ( $N_x = 4$  and  $n = 4$ ).

### 5.3.2. Rectangular membrane with $\mathcal{K} = 2$

Figs. 14 and 15 shows the dimensional natural frequencies of two rectangular ( $\mathcal{N} = 2$ ) membranes with  $\mathcal{K} = 2$  and  $\alpha = 0.1$  and  $\alpha = 0.2$ , respectively (considering  $\beta = \alpha$ ). In these figures, it can be found how the models behave in a similar way to that seen in the previous section, all of them coinciding with the Classic one when  $N_x$  increases, and presenting different performances when it decreases. Analogous to the

previous section, the relative errors of the continuum models, given by Eq. (89), are displayed in Figs. 16 and 17, for  $\alpha = 0.1$  and  $\alpha = 0.2$ , respectively. Here, we can see how the Schrödinger, Regularization and EKE I model are the ones that show the best performance when  $\alpha = 0.1$ , the error of the latter growing when next-nearest interactions become more significant ( $\alpha = 0.2$ ), whereas the Regularization model improves its performance in this case, presenting very low errors at the limit of the IBZ ( $N_x = 4$  and  $m$  or  $n$  equal to 4). Note how the Regularization model shows very small errors around vertex D of the IBZ ( $m = 1, n = 4$  and  $N_x = 4$ ), which has been also verified around the vertex B ( $m = 4, n = 1$  and  $N_x = 4$ ).

## 6. Conclusions

The main goal of this work has been obtaining non-classical continuum models, which reflect the dynamic behaviour of the discrete one as accurately as possible. To this end, different continualization methods have been applied to a membrane lattice system, assessing the performance of the new continuum models by studying both their dispersion relations and the natural frequencies of a fixed-edge configuration. The final conclusions drawn from this work can be summarized as follows.

An equivalent classical membrane model (accounting for long-range forces) is obtained if the scale parameters are disregarded. In addition, it results in the classical membrane model if it is considered that  $b_1 = b_2 = 1$  (neglect of next-nearest interactions).

Standard models accounting for the scale effects present governing equations with high-order spatial derivatives, so they need extra boundary conditions to be solved when dealing with finite (bounded) solids.

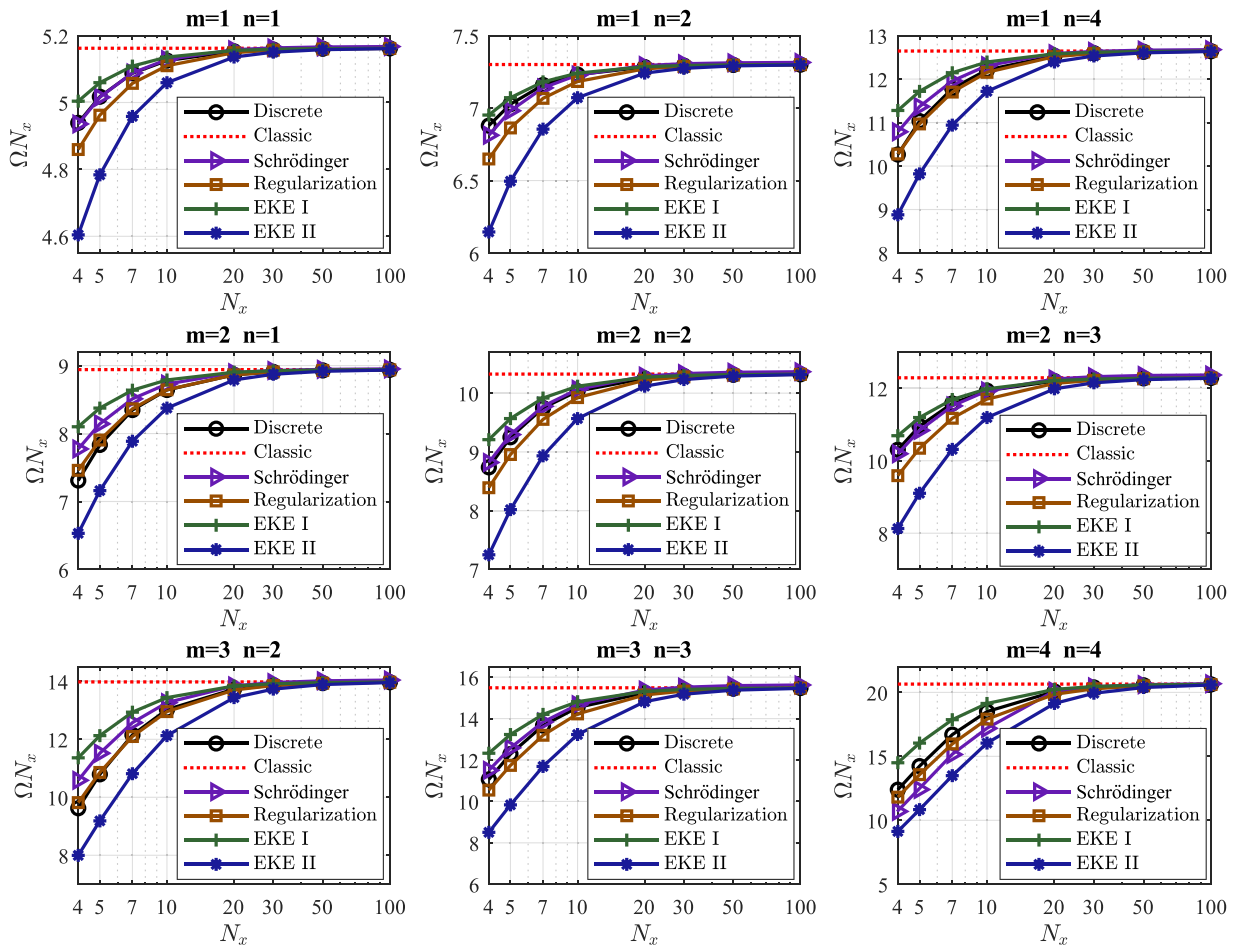


Fig. 15. Dimensionless natural frequencies of a rectangular ( $\mathcal{N} = 2$ ) membrane with  $\mathcal{K} = 2$  for fixed-edge configuration and  $\alpha = \beta = 0.2$ . Representation of continuum and discrete models as a function of  $N_x$ .

Furthermore, these models present some physical inconsistencies for short wavelengths. The Standard I model shows imaginary frequencies for certain wavenumber values, lacking physical sense in a conservative system without any external energy source. On the other hand, the Standard II model does not present a maximum velocity at which disturbances can be propagated, since the modulus of its group velocity tends to infinity in the short-wave limit, regardless of the direction of propagation.

All the problems outlined above can be avoided by the use of non-standard continualization methods, the models derived from them capturing the scaling effects by means of cross derivatives with low spatial order. Moreover, these models include scaling parameters that makes their velocity bounded from above, preventing the appearance of imaginary frequencies. Note also that two scale parameters  $a_3$  and  $a_6$  appear in the Schrödinger model, which affect two derivatives that, although formally of higher order, are of mixed nature thus not requiring the use of extra boundary conditions.

The dispersion curves and the natural frequencies of the square fixed-edge membrane can be correlated, for both the discrete and continuum models, which can be leveraged to know the trend of the dispersion curves along the diagonal of the IBZ (A-B-C-D), through that found in the associated natural frequencies.

We have seen how in finite membranes, size-effects become less relevant as the number of particulates increases (the characteristic length of the lattice system decreases if the same dimensions are kept), the natural frequencies of all modes matching those of the Classic one (scale-length free).

By means of the dispersion analysis, we have seen that, when  $\mathcal{K} = 1$ , the Schrödinger, Regularization and EKE I model are the ones that best capture the behaviour of the discrete model along the limits of the IBZ (sides of the square of vertices A, B, C and D). Moreover, when next-nearest interactions become more relevant ( $\alpha = \beta = 0.2$ ), the error of the Regularization model significantly decreases around vertex C, whereas that of the EKE II model does so around vertices B and D. These performances are similar when  $\mathcal{K} = 2$ , in this case the EKE I model presenting lower errors than for  $\mathcal{K} = 1$ . On the other hand, after the natural frequencies analysis, it had been observed how the EKE I model also captures the behaviour of the discrete one in some areas within the IBZ, their errors increasing when long-range forces become more significant.

To sum up, the continualization of a membrane lattice system with next-nearest interactions has been addressed in this paper, looking for new continuum models that account for size-effects. The novel non-standard models developed can be accepted as suitable approaches to describe wave propagation in such lattices, the Regularization and EKE II models, particularly showing very low errors even for short wavelengths. Interestingly, these models do not present physical inconsistencies and capture the size-effect through cross derivatives with low spatial order.

**CRedit authorship contribution statement**

**F. Gómez-Silva:** Conceptualization, Software, Formal analysis, Writing. **R. Zaera:** Conceptualization, Formal analysis, Writing.

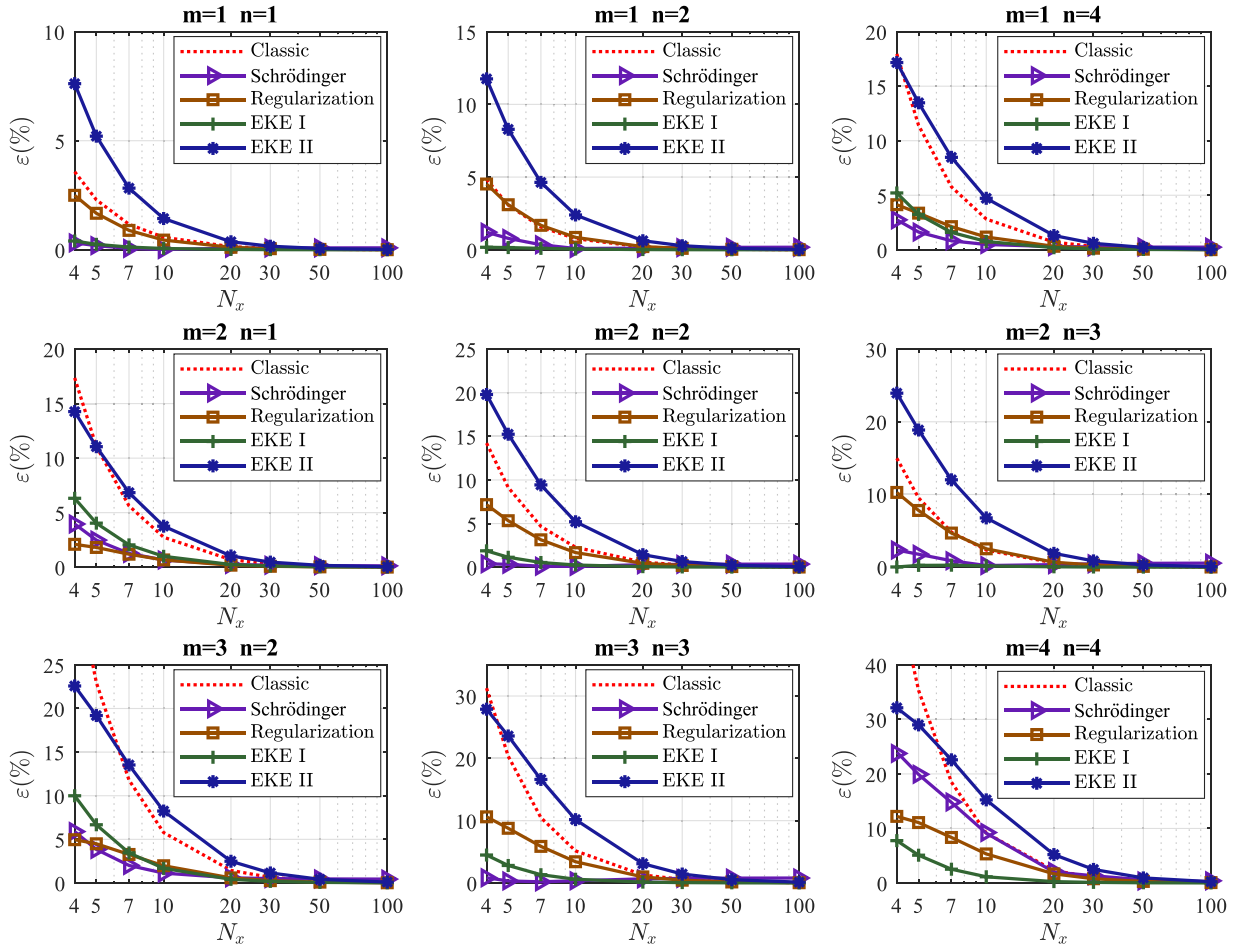


Fig. 16. Relative errors of a rectangular ( $\mathcal{N} = 2$ ) membrane with  $\mathcal{K} = 2$  for fixed-edge configuration and  $\alpha = \beta = 0.1$ . Comparison between continuum models as a function of  $N_x$ .

**Declaration of competing interest**

The authors declare that they have no known competing financial interests or personal relationships that could have appeared to influence the work reported in this paper.

**Data availability**

No data was used for the research described in the article.

**Acknowledgments**

The authors acknowledge support from MCIN/AEI/10.13039/501100011033 under Grants numbers PGC2018-098218-B-I00 and PRE2019-088002. FEDER: A way to make Europe. ESF invests in your future.

**Appendix. Derivation of the enriched kinetic energy densities**

Two different Enriched Kinetic Energy model have been presented in this paper. The first one, EKE I, employs a progressive differences scheme to express the cross spatial derivative, whereas the second one, EKE II, uses a central differences one. Then, both expressions are expanded via Taylor's series leading to

$$\bar{v}_{i,j} \approx Q_l \cdot \bar{v}; \quad l = 1, 2, \tag{A.1}$$

where  $Q_1$  and  $Q_2$  are given by Eqs. (57) and (63), respectively. Hence, the kinetic energy of both models can be continualized as

$$\begin{aligned} \bar{T}_l &= \frac{1}{2} \sum_i \sum_j \left( \frac{\partial \bar{v}_{i,j}}{\partial \tau} \right)^2 = \frac{1}{2} \int_{\Omega} \left[ Q_l \frac{\partial \bar{v}}{\partial \tau} \cdot Q_l \frac{\partial \bar{v}}{\partial \tau} \right] dS \\ &= \frac{1}{2} \int_{\Omega} \left[ \frac{\partial \bar{v}}{\partial \tau} \cdot (Q_l^* Q_l) \frac{\partial \bar{v}}{\partial \tau} \right] dS, \end{aligned} \tag{A.2}$$

where  $Q_l^* = Q_l(-\partial_x, -\partial_y)$  is the adjoint operator of the pseudo-differential operator  $Q_l$ , so

$$Q_1^* Q_1 = 1 - \frac{1}{12} \left( \partial_x^2 + \partial_y^2 \right) + O(\partial_x^4); \tag{A.3}$$

$$Q_2^* Q_2 = 1 - \frac{1}{3} \left( \partial_x^2 + \partial_y^2 \right) + O(\partial_x^4). \tag{A.4}$$

Integrating now by parts the Eq. (A.2), it results in the corresponding expressions

$$\begin{aligned} \bar{T}_1 &= \frac{1}{2} \int_{\Omega} \left[ \left( \frac{\partial \bar{v}}{\partial \tau} \right)^2 + \frac{1}{12} \frac{\partial \bar{v}}{\partial \tau} \left( \frac{\partial^3 \bar{v}}{\partial x^2 \partial \tau} + \frac{\partial^3 \bar{v}}{\partial y^2 \partial \tau} \right) \right] dS = \\ &= \frac{1}{2} \int_{\Omega} \left[ \left( \frac{\partial \bar{v}}{\partial \tau} \right)^2 + \frac{1}{12} \left( \left( \frac{\partial^2 \bar{v}}{\partial x \partial \tau} \right)^2 + \left( \frac{\partial^2 \bar{v}}{\partial y \partial \tau} \right)^2 \right) \right] dS - \frac{1}{2} \int_{\partial \Omega} \frac{\partial \bar{v}}{\partial \tau} \nabla \left( \frac{\partial \bar{v}}{\partial \tau} \right) \cdot \bar{n} dS; \end{aligned} \tag{A.5}$$

$$\begin{aligned} \bar{T}_2 &= \frac{1}{2} \int_{\Omega} \left[ \left( \frac{\partial \bar{v}}{\partial \tau} \right)^2 + \frac{1}{3} \frac{\partial \bar{v}}{\partial \tau} \left( \frac{\partial^3 \bar{v}}{\partial x^2 \partial \tau} + \frac{\partial^3 \bar{v}}{\partial y^2 \partial \tau} \right) \right] dS = \\ &= \frac{1}{2} \int_{\Omega} \left[ \left( \frac{\partial \bar{v}}{\partial \tau} \right)^2 + \frac{1}{3} \left( \left( \frac{\partial^2 \bar{v}}{\partial x \partial \tau} \right)^2 + \left( \frac{\partial^2 \bar{v}}{\partial y \partial \tau} \right)^2 \right) \right] dS - \frac{1}{2} \int_{\partial \Omega} \frac{\partial \bar{v}}{\partial \tau} \nabla \left( \frac{\partial \bar{v}}{\partial \tau} \right) \cdot \bar{n} dS, \end{aligned}$$

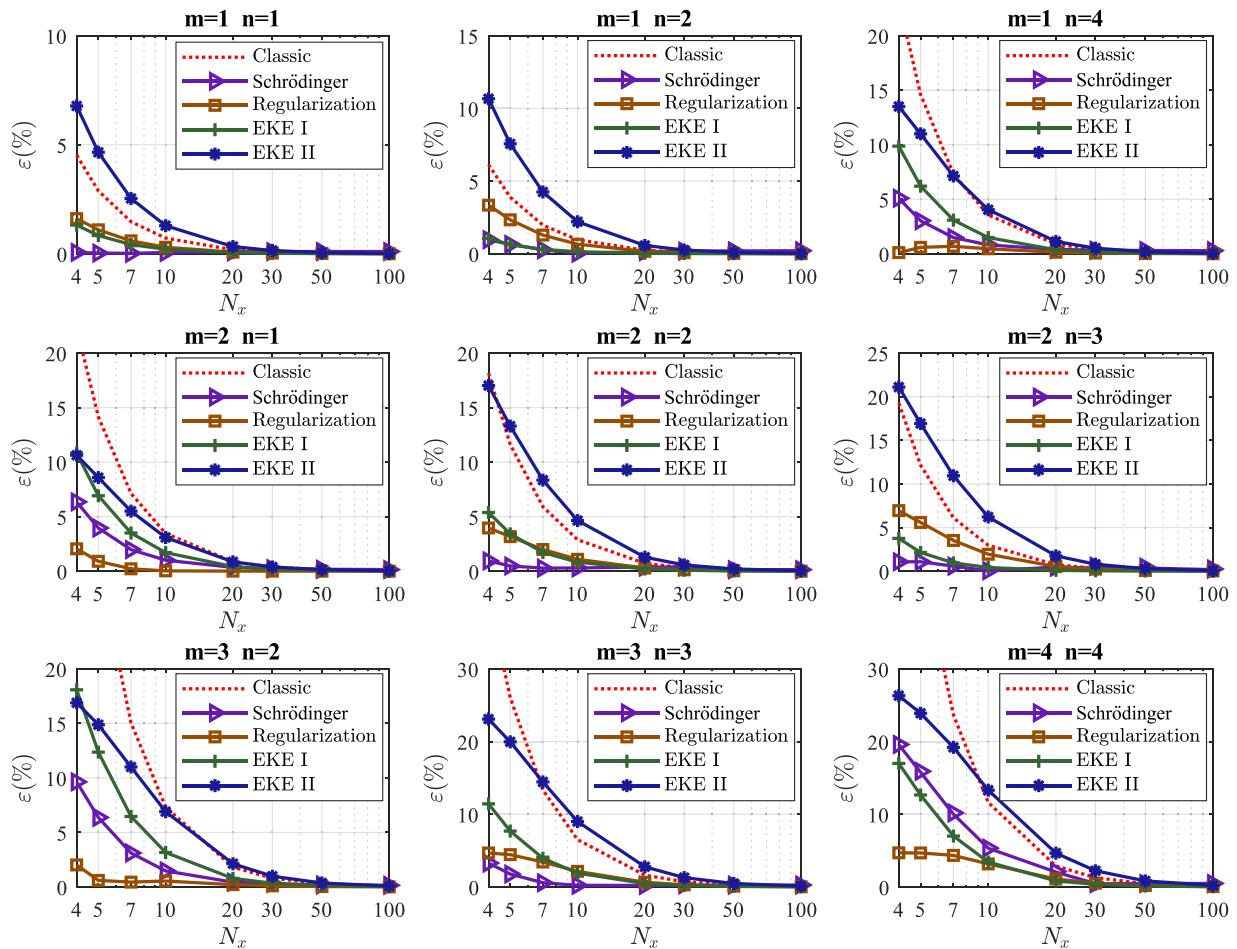


Fig. 17. Relative errors of a rectangular ( $\mathcal{N} = 2$ ) membrane with  $\mathcal{K} = 2$  for fixed-edge configuration and  $\alpha = \beta = 0.2$ . Comparison between continuum models as a function of  $N_x$ .

$$(A.6)$$

where  $\vec{n} = (n_x, n_y)$  is the vector normal to the edge. Taking into account that the boundary terms of Eqs. (A.5) and (A.6) do not play any role when applying Hamilton's Principle, the next expressions for the Enriched Kinetic Energy densities can be assumed

$$\bar{T}_1 = \frac{1}{2} \left[ \left( \frac{\partial \bar{v}}{\partial \tau} \right)^2 + \frac{1}{12} \left( \left( \frac{\partial^2 \bar{v}}{\partial \bar{x} \partial \tau} \right)^2 + \left( \frac{\partial^2 \bar{v}}{\partial \bar{y} \partial \tau} \right)^2 \right) \right]; \tag{A.7}$$

$$\bar{T}_2 = \frac{1}{2} \left[ \left( \frac{\partial \bar{v}}{\partial \tau} \right)^2 + \frac{1}{3} \left( \left( \frac{\partial^2 \bar{v}}{\partial \bar{x} \partial \tau} \right)^2 + \left( \frac{\partial^2 \bar{v}}{\partial \bar{y} \partial \tau} \right)^2 \right) \right], \tag{A.8}$$

both of them being positive definite.

References

Abdelrahman, A.A., Esen, I., Özarpa, C., Eltaher, M.A., 2021. Dynamics of perforated nanobeams subject to moving mass using the nonlocal strain gradient theory. *Appl. Math. Model.* 96, 215–235.

Andrianov, I., 2002. The specific features of the limiting transition from a discrete elastic medium to a continuous one. *J. Appl. Math. Mech.* 66, 261–265.

Andrianov, I., Awrejcewicz, J., 2003. On the average continuous representation of an elastic discrete medium. *J. Sound Vib.* 264, 1187–1194.

Andrianov, I.V., Awrejcewicz, J., 2005. Continuous models for chain of inertially linked masses. *Eur. J. Mech. A Solids* 24, 532–536.

Andrianov, I., Awrejcewicz, J., 2008. Continuous models for 2D discrete media valid for higher-frequency domain. *Comput. Struct.* 86, 140–144.

Andrianov, I., Awrejcewicz, J., Weichert, D., 2010. Improved continuous models for discrete media. *Math. Probl. Eng.* 2010, 1–35.

Andrianov, I., Koblik, S., Starushenko, G., 2021. Transition from discrete to continuous media: The impact of symmetry changes on asymptotic behavior of waves. *Symmetry* 13, 1008.

Bacigalupo, A., Gambarotta, L., 2019. Generalized micropolar continualization of 1D beam lattices. *Int. J. Mech. Sci.* 155, 554–570.

Bacigalupo, A., Gambarotta, L., 2021. Identification of non-local continua for lattice-like materials. *Internat. J. Engrg. Sci.* 159, 103430.

Barretta, R., Faghidian, S.A., Luciano, R., 2019. Longitudinal vibrations of nano-rods by stress-driven integral elasticity. *Mech. Adv. Mater. Struct.* 26, 1307–1315.

Braun, T., Barwich, V., Ghatkesar, M.K., Bredekamp, A.H., Gerber, C., Hegner, M., Lang, H.P., 2005. Micromechanical mass sensors for biomolecular detection in a physiological environment. *Phys. Rev. E* 72, 031907.

Caldas, E.M., Novatzky, D., Deon, M., de Menezes, E.W., Hertz, P.F., Costa, T.M.H., Arenas, L.T., Benvenuti, E.V., 2017. Pore size effect in the amount of immobilized enzyme for manufacturing carbon ceramic biosensor. *Microporous Mesoporous Mater.* 247, 95–102.

Challamel, N., Aydogdu, M., Elishakoff, I., 2018. Statics and dynamics of nanorods embedded in an elastic medium: Nonlocal elasticity and lattice formulations. *Eur. J. Mech. A Solids* 67, 254–271.

Challamel, N., Zhang, Z., Wang, C., Reddy, J., Wang, Q., Michelitsch, T., Collet, B., 2014. On nonconservativeness of Eringen's nonlocal elasticity in beam mechanics: correction from a discrete-based approach. *Arch. Appl. Mech.* 84, 1275–1292.

Civalek, Ö., Dastjerdi, S., Akbaş, Ş.D., Akgöz, B., 2021. Vibration analysis of carbon nanotube-reinforced composite microbeams. *Math. Methods Appl. Sci.* 1–17.

Di Paola, M., Failla, G., Zingales, M., 2010. The mechanically-based approach to 3D non-local linear elasticity theory: Long-range central interactions. *Int. J. Solids Struct.* 47, 2347–2358.

Duan, W.H., Challamel, N., Wang, C., Ding, Z., 2013. Development of analytical vibration solutions for microstructured beam model to calibrate length scale coefficient in nonlocal Timoshenko beams. *J. Appl. Phys.* 114, 104312.

Dunn, M., Wheel, M., 2020. Size effect anomalies in the behaviour of loaded 3D mechanical metamaterials. *Philos. Mag. (Series 8)* 100, 139–156.

Eom, K., Park, H.S., Yoon, D.S., Kwon, T., 2011. Nanomechanical resonators and their applications in biological/chemical detection: nanomechanics principles. *Phys. Rep.* 503, 115–163.

Eringen, A.C., 1966. Linear theory of micropolar elasticity. *J. Math. Mech.* 15, 909–923.

Eringen, A.C., Edelen, D., 1972. On nonlocal elasticity. *Internat. J. Engrg. Sci.* 10, 233–248.

- Gaziz, D., Wallis, R., 1965. Surface tension and surface modes in semi-infinite lattices. *Surf. Sci.* 3, 19–32.
- Gómez-Silva, F., Fernández-Sáez, J., Zaera, R., 2020. Nonstandard continualization of 1D lattice with next-nearest interactions. Low order ODEs and enhanced prediction of the dispersive behavior. *Mech. Adv. Mater. Struct.* 1–10.
- Gómez-Silva, F., Zaera, R., 2021. Analysis of low order non-standard continualization methods for enhanced prediction of the dispersive behaviour of a beam lattice. *Int. J. Mech. Sci.* 196, 1–11.
- Gómez-Silva, F., Zaera, R., 2022. Low-order non-classical continuum models for the improved prediction of an anisotropic membrane lattice's dynamics. *Thin-Walled Structures* 179, 109632.
- Gómez-Silva, F., Zaera, R., 2022a. Dynamic analysis and non-standard continualization of a Timoshenko beam lattice. *Int. J. Mech. Sci.* 214, 106873.
- Gómez-Silva, F., Zaera, R., 2022b. Novel Enriched Kinetic Energy continuum model for the enhanced prediction of a 1D lattice with next-nearest interactions. *Compos. Struct.* 281, 115003.
- Hache, F., Challamel, N., Elishakoff, I., Wang, C., 2017. Comparison of nonlocal continualization schemes for lattice beams and plates. *Arch. Appl. Mech.* 87, 1105–1138.
- Harbola, V., Crossley, S., Hong, S.S., Lu, D., Birkholzer, Y.A., Hikita, Y., Hwang, H.Y., 2021. Strain gradient elasticity in SrTiO<sub>3</sub> membranes: Bending versus stretching. *Nano Lett.* 21, 2470–2475.
- Hérissou, B., Challamel, N., Picandet, V., Perrot, A., Wang, C., 2018. Static and dynamic behaviors of microstructured membranes within nonlocal mechanics. *J. Eng. Mech.* 144, 04017155.
- Khakalo, S., Niiranen, J., 2018. Form II of mindlin's second strain gradient theory of elasticity with a simplification: For materials and structures from nano-to macro-scales. *Eur. J. Mech. A Solids* 71, 292–319.
- Kunin, I.A., 2012. *Elastic Media with Microstructure I: One-Dimensional Models*, Vol. 26. Springer Science & Business Media.
- Lee, D., Nguyen, D.M., Rho, J., 2017. Acoustic wave science realized by metamaterials. *Nano Convergence* 4, 3.
- Liu, C., Yu, J., Xu, W., Zhang, X., Wang, X., 2021. Dispersion characteristics of guided waves in functionally graded anisotropic micro/nano-plates based on the modified couple stress theory. *Thin-Walled Struct.* 161, 1–11.
- Lombardo, M., Askes, H., 2010. Elastic wave dispersion in microstructured membranes. *Proc. R. Soc. A: Math. Phys. Eng. Sci.* 466, 1789–1807.
- Maslov, V.P., 1976. *Operational Methods*. Mir.
- Metrikine, A.V., Askes, H., 2002. One-dimensional dynamically consistent gradient elasticity models derived from a discrete microstructure: Part I: Generic formulation. *Eur. J. Mech. A Solids* 21, 555–572.
- Mindlin, R.D., 1963. *Microstructure in linear elasticity*. Tech. rep., Columbia Univ., New York, Dept. of Civil Engineering and Engineering Mechanics.
- Mindlin, R., 1965. On the equations of elastic materials with micro-structure. *Int. J. Solids Struct.* 1, 73–78.
- Papkova, I., Yakovleva, T., Krysko, A., Krysko, V., 2022. Nonlinear dynamics of NEMS/MEMS elements in the form of beams taking into account the temperature field, radiation exposure, elastoplastic deformations. In: *Advances in Nonlinear Dynamics*. Springer, pp. 311–320.
- Polyzos, D., Fotiadis, D., 2012. Derivation of Mindlin's first and second strain gradient elastic theory via simple lattice and continuum models. *Int. J. Solids Struct.* 49, 470–480.
- Rafiee, M., Nitzsche, F., Labrosse, M., 2017. Dynamics, vibration and control of rotating composite beams and blades: A critical review. *Thin-Walled Struct.* 119, 795–819.
- Rahmani, A., Faroughi, S., Sari, M., Abdelkefi, A., 2022. Selection of size dependency theory effects on the wave's dispersions of magneto-electro-thermo-elastic nano-beam resting on visco-elastic foundation. *Eur. J. Mech. A Solids* 104620.
- Rosenau, P., 1987. Dynamics of dense lattices. *Phys. Rev. B* 36, 5868.
- Rosenau, P., 2003. Hamiltonian dynamics of dense chains and lattices: or how to correct the continuum. *Phys. Lett. A* 311, 39–52.
- Shang, Y., Qian, Z.-H., Cen, S., Li, C.-F., 2019. A simple unsymmetric 4-node 12-DOF membrane element for the modified couple stress theory. *Internat. J. Numer. Methods Engrg.* 119, 807–825.
- Shubin, M.A., 1987. *Pseudodifferential Operators and Spectral Theory*, Vol. 57. Springer.
- Thai, C.H., Ferreira, A., Rabczuk, T., Nguyen-Xuan, H., 2018. Size-dependent analysis of FG-CNTRC microplates based on modified strain gradient elasticity theory. *Eur. J. Mech. A Solids* 72, 521–538.
- Toupin, R., 1962. Elastic materials with couple-stresses. *Arch. Ration. Mech. Anal.* 11, 385–414.
- Wang, C., Zhang, Z., Challamel, N., Duan, W., 2013. Calibration of eringen's small length scale coefficient for initially stressed vibrating nonlocal Euler beams based on microstructured beam model. *J. Phys. D: Appl. Phys.* 46, 345501.
- Wisnom, M., 1999. Size effects in the testing of fibre-composite materials. *Compos. Sci. Technol.* 59, 1937–1957.
- Yin, Y.M., Li, H.Y., Xu, J., Zhang, C., Liang, F., Li, X., Jiang, Y., Cao, J.W., Feng, H.F., Mao, J.N., Qin, L., Kang, Y.F., Zhu, G., 2021. Facile fabrication of flexible pressure sensor with programmable lattice structure. *ACS Appl. Mater. Interfaces* 13, 10388–10396.
- Zaera, R., Vila, J., Fernández-Sáez, J., Ruzzene, M., 2018. Propagation of solitons in a two-dimensional nonlinear square lattice. *Int. J. Non-Linear Mech.* 106, 188–204.
- Zhang, Z., Challamel, N., Wang, C., 2013. Eringen's small length scale coefficient for buckling of nonlocal Timoshenko beam based on microstructured beam model. *J. Appl. Phys.* 114, 114902.
- Zhang, B., Li, H., Kong, L., Shen, H., Zhang, X., 2020. Coupling effects of surface energy, strain gradient, and inertia gradient on the vibration behavior of small-scale beams. *Int. J. Mech. Sci.* 184, 1–21.